Lethaia
AN INTERNATIONAL JOURNAL OF PALAEONTOLOGY AND STRATIGRAPHY

Fossil fish provide evidence of geomelanin preservation with implications on the visual accuracy of an extinct fish species

GUSTAVO PRADO, RAFAEL C.J.P.S. SALVATO, BRUNO BECKER-KERBER, EVANDRO P. SILVA, FELIPE L. PINHEIRO, GABRIEL L. OSÉS, DOUGLAS GALANTE, FABIO RODRIGUES, JAIME J. DIAS, ISMAR DE SOUZA CARVALHO, EVAN T. SAITTA, LUCAS M. LINO AND LUIZ E. ANELLI

LETHAIA

Eumelanin is a ubiquitous type of pigment, standing present in all major life branches. Chemically, it consists of 5,6-dihydroxyindole (DHI) and 5,6-dihydroxyindole-2-carboxylic acid (DHICA) units bonded with varied functional groups. This biochrome is involved in many different roles, such as free radical scavenging, microbial inhibition, etc. Eumelanin is produced by organelles called melanosomes, which are found throughout the animals' body. In the fish's eyes, this pigment mainly plays a protective role against UV radiation damage and waterborne insults. The previous detection of melanosomes in the eyes of fossil teleosts already provided evidence for the palaeobiology and palaeoecology of extinct fish lineages. Nonetheless, the presence of these organelles remains to be detected in exceptionally preserved fossils from Brazil. Here, we report the microscopic and chemical investigation of fossil melanin from the eyes of the Cretaceous fish *Dastilbe crandalli*. Results show that the eye has a circular shape with non-recalcitrant dark brown tissues at its rims, exhibiting densely packed, solid, subspherical micrometric granules rich in carbon and with vibrational spectra of eumelanin. Geothermic calculations of the Raman spectra indicate that melanin is not much thermally altered. This result is consistent with other proposals for the maximum temperature for this unit, raising the possibility of its use to estimate the thermal alteration of geomelanins. Besides that, these results also indicate that *Dastilbe* fish possibly had a limited visual capability or lived in the shallow but shadowed (by aquatic plants) portions of the palaeolake. □ *Melanin, Raman Spectroscopy, Cretaceous, Crato Formation.*

Gustavo M.E.M. Prado ✉ [gustavo.marcondes.prado@usp.br], Laboratory of Chemosphere, Institute of Chemistry, University of São Paulo, São Paulo, Brazil, Institute of Geosciences, University of Sao Paulo, Sao Paulo, Brazil; Douglas Galante [galante@usp.br], Lucas M. Lino [lucas.martins.santos@usp.br] and Luiz E. Anelli [anelli@usp.br], Institute of Geosciences, University of São Paulo, São Paulo, Brazil; Rafael C.J.P.S. Salvato [rafaelcaetano@usp.br], School of Engineering of Lorena, University of São Paulo, Lorena, São Paulo, Brazil; Bruno Becker-Kerber [beckerkerber@gmail.com], Institute of Geosciences, University of São Paulo, São Paulo, Brazil and Brazilian Synchrotron Light Laboratory, Centre for Research in Energy and Materials, Campinas, São Paulo, Brazil; Evandro P. Silva [evandro.pereira.silva@usp.br] and Fabio Rodrigues [farod@iq.usp.br], Laboratory of Chemosphere, Institute of Chemistry, University of São Paulo, São Paulo, Brazil; Felipe L. Pinheiro [felipepinheiro@unipampa.edu.br], Laboratory of Palaeobiology, Federal University of Pampa, São Gabriel, Rio Grande do Sul, Brazil; Gabriel L. Osés [gabriel.oses@alumni.usp.br], Laboratory of Archaeometry and Sciences Applied to Cultural Heritage, Institute of Physics, University of São Paulo, São Paulo, Brazil; Jaime J. Dias [jaimejoaquimdias@gmail.com], Geology Department, Federal University of Rio de Janeiro, Rio de Janeiro, Brazil; Ismar de Souza Carvalho [ismar@geologia.ufrj.br], Geology Department, Federal University of Rio de Janeiro, Rio de Janeiro, Brazil and Centre of Geosciences, Coimbra University, Portugal; Evan T. Saitta [evansaitta@gmail.com], Life Sciences Section, Negaunee Integrative Research Center, Field Museum, Chicago, Illinois, USA; *manuscript received on 17/06/2024; manuscript accepted on 21/04/2025; manuscript published on 12/08/2025 in Lethaia 58*(3).

Since the early evolution of animals, many species have developed numerous adaptations to help them to survive a vast array of environmental conditions (Cuthill *et al.* 2017). In fish, some of the most notable are the development of the cup-type eye with a moveable lens to focus objects and photoreceptor cells that allows for the recognition of colours (Land 2014). Because water scatters and diffuses light (Land 2014), the ability to effectively recognize underwater objects and to perceive colours and shades in dim light conditions is crucial for survival and reproduction in fish (e.g. Davis *et al.* 2020).

The colour patterns of fish are produced by the presence and distribution of natural pigments (Roy *et al.* 2020a), and these expressions are produced by multiple kinds of biochromes, such as carotenoids, guanine, pterin, and melanin. Among these pigments, melanin is ubiquitous in all domains of life occurring in tissues

https://doi.org/10.18261/let.58.3.7

of Archaea, Bacteria, and Eukaryotes (Borovanský & Riley 2011; Ma & Sun 2012; D'Alba & Shawkey 2019). Although varied chemical types of melanin exist, this compound consists of several pyrrolic and phenolic rings, bonded with varied functional groups and organometallic compounds (Powell *et al.* 2004; Kaxiras *et al.* 2006; *Meredith et al.* 2006; Tran *et al.* 2006; Watt *et al.* 2009; Bellono & Oancea 2014; Prampolini *et al.* 2015). Due to its many π-π carbon bonds and the presence of carbonyls, hydroxyls, and thiols, this pigment is highly reactive to free ions, aiding in cellular protection, with antioxidant and antibacterial effects (Różanowska *et al.* 1999; Mackintosh 2001). Given its high chemical heterogeneity and wide distribution in terms of organismal expression, the precise molecular structure of most melanins remains largely obscure (d'Ischia *et al.* 2013; Solano 2014).

Melanogenesis is a series of chemical reactions that produce two major types of melanin: the black to brown carbonyl-rich eumelanin and the reddish to yellowish cysteine-rich phaeomelanin. Between these two categories, the former is the most common, being present, though in small quantities, even in tissues rich with the later compound (Ito 2003; Ito & Wakamatsu 2008; Ito *et al.* 2011; d'Ischia *et al.* 2013; Solano 2014; Ito *et al.* 2017; Wakamatsu *et al.* 2017). Most studies agree with the Raper-Mason pathway model for the synthesis of eumelanin (Solano 2014), and this biochemical cascade begins with the oxidation of the amino acid tyrosine and ends with the production of the two direct precursors; the 5,6-dihydroxyindole (DHI) and 5,6,-dihydroxyindole-2-carboxylic acid (DHICA) (Xiao *et al.* 2018; Ni *et al.* 2020). The synthesis of eumelanin occurs inside melanosomes, a lysosome-related organelle that originates from specialised cells called melanocytes or melanophores (Wasmeier *et al.* 2008, Solano 2014). Due to the diverse organization of the melanin grains inside the melanosomes, these subcellular structures can assume various morphologies, including a solid or hollowed granule with cylindrical, flat, spherical, or oblate shapes (Nordén *et al.* 2018). The development and abundance of these microbodies and melanin content is directly associated to the level of colour saturation of the tissues they are deposited in (Solano 2014). Hence, it is not surprising that melanosomes can be found in modern and fossil skin, feathers, hairs, eyes, and internal organs (McNamara *et al.* 2018).

It is generally accepted that, in fossils, phaeomelanin is usually absent or significantly altered due to its less stable nature, whereas eumelanin is found in most exceptionally preserved specimens, although also occurring chemically slightly altered (Glass *et al.* 2012, 2013; Colleary *et al.* 2015; Manning *et al.* 2019; Jarenmark *et al.* 2021; Umamaheswaran *et al.* 2021, 2022). The loss of carboxylic acids and extensive crosslinking also lead to conversion of melanin into an 'aged melanin' (Ito *et al.* 2013), or in other words, 'geomelanins' (Vinther 2020; Roy *et al.* 2023). Aside from that, the identification of ancient biochromes and their ultrastructure can also provide information on the paleoenvironmental and taphonomic conditions that acted on fossil preservation (Briggs & Summons 2014; Parry *et al.* 2017).

In Brazil, melanosomes have been formally identified in isolated feathers (Vinther *et al.* 2008; Campos *et al.* 2019) and pterosaur soft tissues (Pinheiro *et al.* 2019; Cincotta *et al.* 2022), all reported from the Cretaceous Crato Formation *Lagerstätte*. Conspicuously, in a previous study (Osés *et al.* 2017), none of these microbodies were found in the tissues of the fish *Dastilbe crandalli* Jordan 1910. Here, we report the results of a microscopic and chemical investigation on the remains of a preserved fish eye from a specimen from the same species from the Cretaceous Crato Formation (Araripe Basin, NE Brazil). This specimen exhibits the presence of numerous and physically intact sub-spherical microbodies that are consistent with melanosomes. We discuss the presence of these micro-sized particles in addition to the fossilization of melanin by estimating the temperature of thermal alteration by the means of spectral processing. As a result, through this study, we introduce a new cheaper, and fast approach to study the fossilization of this biochrome which may be useful on understanding of the chemical behaviour and taphonomic history of this pigment.

Geological setting

Located in northeastern Brazil (Fig. 1A), the Crato Formation is part of the Mesozoic intrabasinal sequence of the Araripe Basin (Fig. 1B), cropping out in the states of Ceará, Pernambuco, and Piauí (Assine *et al.* 2014). The Crato Formation (Fig. 1C, D), consists of fossiliferous limestones, shales, sandstones, and fine laminae of evaporites deposited mainly in a hypersaline lacustrine (Warren *et al.* 2017) and wetland systems (Ribeiro *et al.* 2021), under an arid climate (Bernardes-de-Oliveira *et al.* 2014). The age of the Crato Formation (Fig 1E) is based on microfossil and pollen content that indicates an Alagoas Stage (P-270), which partially corresponds to the Aptian, ca. 110 Ma (Coimbra *et al.* 2002; Rios-Netto *et al.* 2012; Arai & Assine 2020; Melo *et al.* 2020; Coimbra & Freire 2021; Guzmán *et al.* 2023; Santos Filho *et al.* 2023).

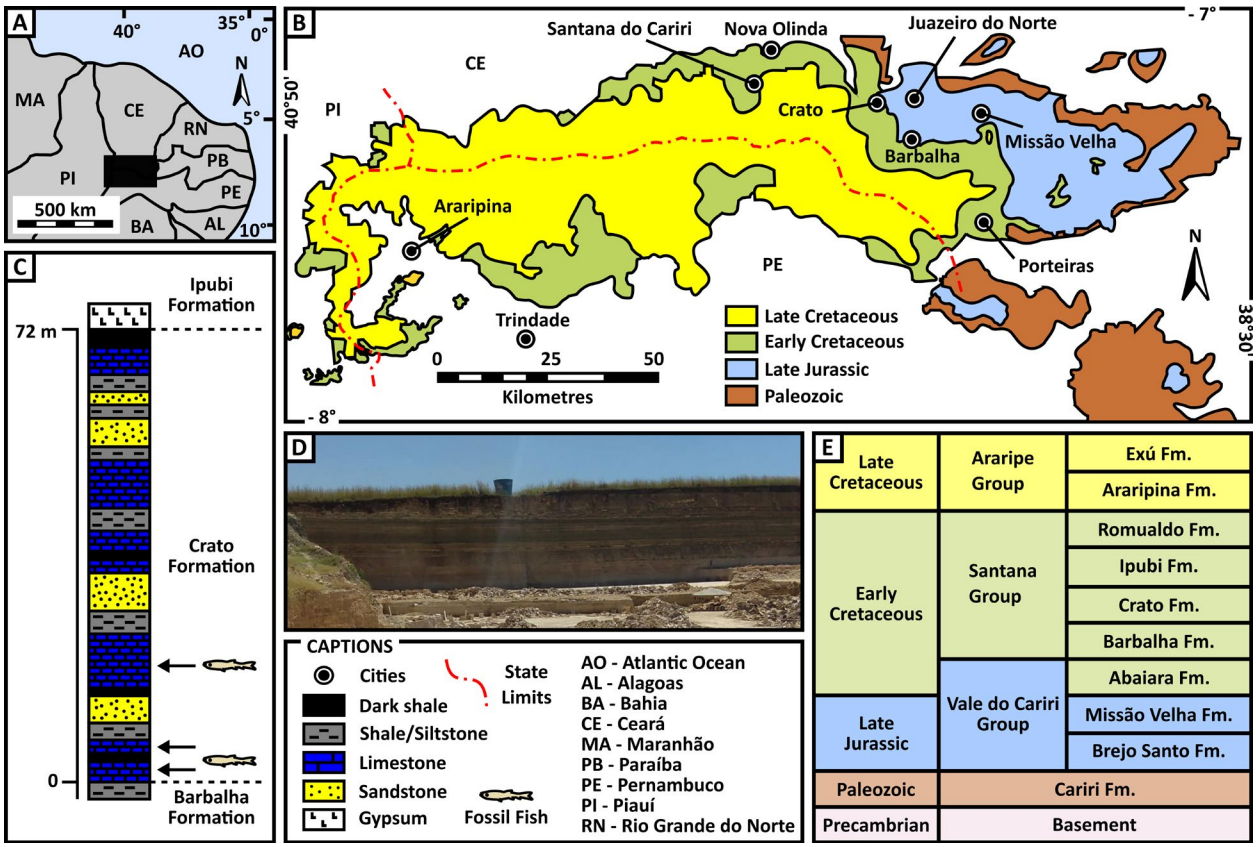

Fig. 1. The location of the Araripe Basin and the Crato Formation beds. A, the geographical region of the Araripe Basin. This basin is located in the northeastern part of Brazil (black rectangle) where it crops out in the Piauí, Ceará and Pernambuco states. B, lithostratigraphical distribution of the Araripe Basin. C, lithostratigraphical column of the Crato Formation based on the well-logs representative of the middle of the basin where most rocks can be found. D, photo of the Crato Formation outcrop (Mina da Pedra Branca, Nova Olinda-CE). E, chronostratigraphical chart of the Araripe Basin units. A and B were taken in Pinheiro *et al.* (2019: CCBY 4.0). C is based on the works of Catto *et al.* (2016) and Varejão *et al.* (2019).

The carbonate beds were formed by the contribution of microorganisms and the lack of trace fossils or evidence of significant bottom currents suggests that carbonate was deposited in calm bottom water under reducing conditions (Heimhofer *et al.* 2010; Catto *et al.* 2016; Warren *et al.* 2017; Varejão *et al.* 2019). The Crato Formation is world famous for its rich and exceptionally preserved biota consisting of various groups of microfossils, plants, and animals (Martill *et al.* 2007; Mendes *et al.* 2021; Ribeiro *et al.* 2020), whose preservation was induced by microbial mats (Carvalho *et al.* 2015; Osés *et al.* 2016, 2017; Varejão *et al.* 2019; Prado *et al.* 2021; Dias *et al.* 2022, 2023). The abundant fossils often appear preserving soft tissues in three dimensions, such as muscle fibres, digestive and reproductive system, among others, a feature that allowed this unit to be recognized as a *Konservat-Lagerstätte* (Dias & Carvalho 2020; Dias *et al.* 2023; Storari *et al.* 2024).

Material and methods

The fossil studied here is an incomplete but partially articulated specimen of the fish *Dastilbe crandalli* Jordan, 1910 (Fig. 2; SOM1, Fig. S1, A), preserved in a buff-coloured limestone matrix (see the taxonomic discussion in SOM1, Fig. S1). Although the precise taxonomic identification of this fish fossil was not the focus of this study, due to the readily observed characters of the bones, the specimen's body size, and the fact that *Dastilbe* is the most abundant species in the Crato beds (Davis & Martill 1999), the probability that this specimen represents this taxon is high. Soft tissues appear as dark brown matter that is limited to discrete regions (SOM1, Fig. S1 B-C), and is distinct from bones that are light brown/beige hue. The fossil comes from Crato Formation beds and is housed in the Palaeontological Collection of the Institute of Geosciences of the University of São Paulo (IGc-USP)

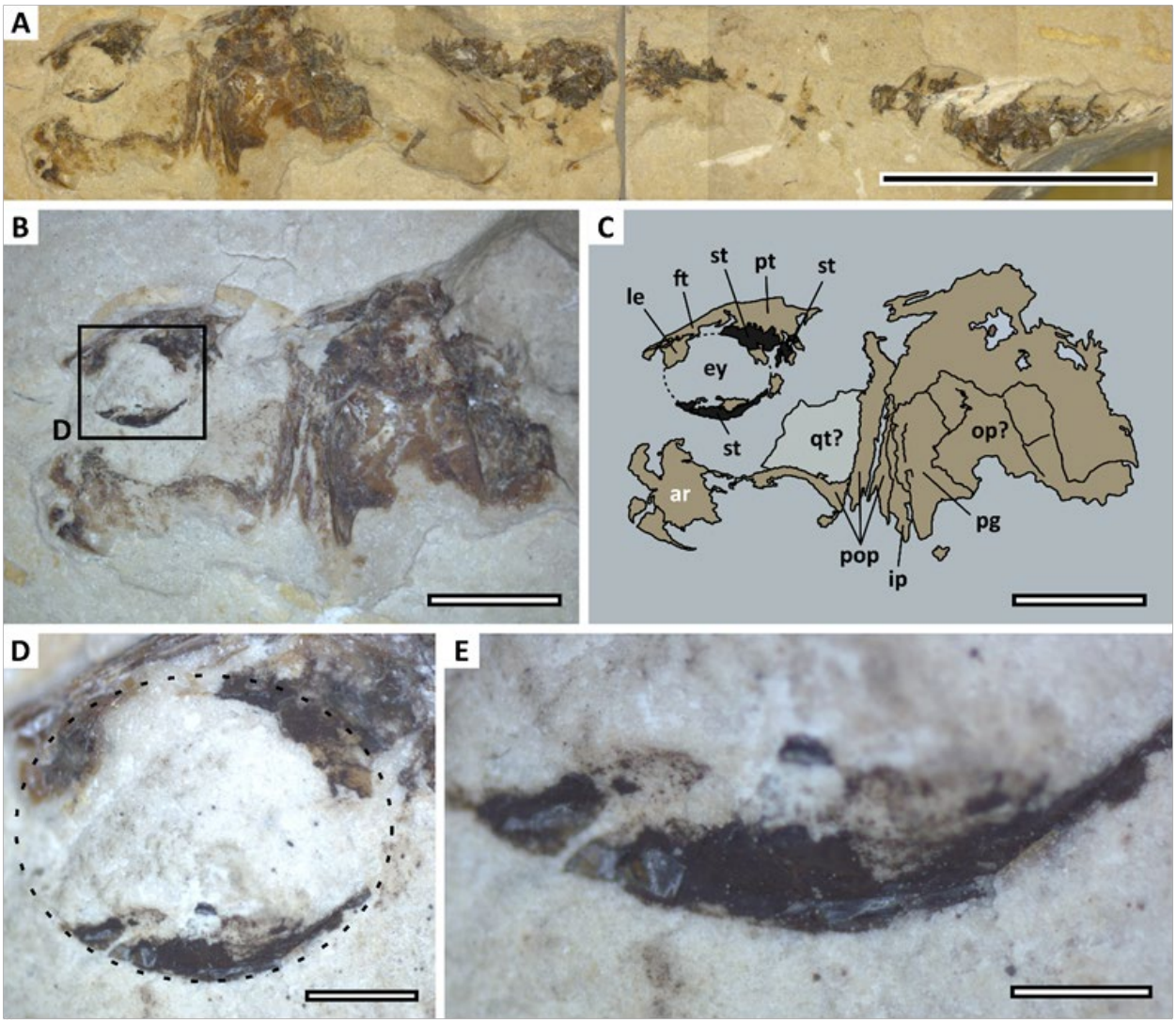

Fig. 2. The analysed fossil fish. A, the whole specimen. B, magnified view of the head. C, interpretative drawing of the head (seen in A) with tentative identification of bony structures (dark beige) and soft tissues around the eye (in black). D, detail of the eye showing its circular shape (black dashed line). E, detail of the lower rim of the eye showing the presence of an amorphous dark brown material. Abbreviations in (C): (ar) articular, (ey) eye, (ft) frontal, (ip) interopercle, (le) lateral ethmoid, (op) opercle, (pop) preopercle, (pt) parietal, (qt) quadrate, (st) soft tissue. Scale bars: (A) 10 mm, (B and C) 4 mm, (D) 1 mm, (E) 500 μm.

with the collection number GP/2E-9378b. No special permits were necessary to perform the study, and the fossil eye was examined in optical stereomicroscope (OM), confocal microscope (COM), and scanning electron microscope (SEM). Elemental composition was identified using energy dispersive spectroscopy (EDS). Microbodies identified in SEM were measured from micrographs using ImageJ 1.50i software (Schneider *et al.* 2012), while descriptive statistics, Mixture Modelling, and their respective graphs were computed in the software Excel, Origin 2022 (OriginLab Co., Northampton, MA, USA), PAST (Hammer *et al.* 2001), and JMP 16.2.0 (SAS Institute Inc., Cary, NC, USA). Raman spectroscopy (RS) and Fourier-Transform Infrared spectroscopy (FTIR) were used to obtain the molecular information (SOM2, Tables S1-S5). To compare the Raman spectra from the fossil fish eye, we also analysed a synthetic melanin and *Sepia* melanin (Sigma-Aldrich, Saint Louis, MO, USA), and a natural released contour feather of a helmeted guineafowl (*Numida meleagris*). Assuming that melanins of fossils may undergo similar chemical processes during diagenesis as do other organic biomolecules, the temperature of alteration of melanin-derived kerogen could also be estimated using more stablished Raman parameters.

To investigate this, we used the more reliable Raman parameters of full width at half maximum of the G-function (G-FWHM) and the Raman band separation (RBS), but we also included R1 (D1 height/G height), D1-FWHM and $D1_A/G_A$ (D1 area/G area) and Kouketsu *et al.* (2014) equation (SOM2: Tab. S6). All spectra were obtained and processed using the software Wire (Renishaw plc., Gloucestershire, UK), Fityk 1.3.1, and Origin 2022, and all figures were made using the software Inkscape™ 0.92. For further material and methods details, as well as spectroscopic data, see Supplementary Material (SOM1, SOM2).

Results

Under the OM, the fish eye (Fig. 2) exhibits a circular shape (Fig. 2D) with a dark brown amorphous substance at the upper and lower rims (Fig. 2E) with a white colour in the centre. The amorphous matter bony tissues stands out by its darker hue (Fig. 2B, C) that contrasts with the beige hue of the bones and whitish colouration of the matrix. The COM images of the rims show that the brown material is typical in appearance to carbonaceous compounds (Muscente *et al.* 2018). This dark material exhibits a grainy texture, with a dense pack of shiny micrometric globules (Fig. 3A). In contrast, the host matrix has only anhedral and blocky rhombohedral crystals with white-grey colour (Fig. 3B), which is common in the Crato Formation laminated limestones (Heimhofer *et al.* 2010).

The SEM investigation provides further support for the COM images, indicating that the rims are formed by solid subspherical particles (Fig. 3C-E), with regular size, smooth surface and high density (Fig. 3F). Although spherules can be also found in the central eye region, they are highly scattered and scarce, suggesting that most have been lost and/or remained in the counterpart, or that their concentration was originally lower. Although they are the most abundant shape in the dark regions of the eye rims, a few elongated microbodies can be also found, though in lower density (Fig. 3G). Altogether, the eye microbodies exhibit a fairly consistent size, subspherical shape, smooth surface, and high density. In contrast, the matrix is composed mainly of subhedral to euhedral blocky and tiny crystals, lacking the spherical microbodies (Fig. 3H).

The overall dimensions of these microbodies exhibit an estimated size of 0.632 ± 0.172 μm in length and 0.489 ± 0.135 μm in width (n = 1593), with a mean aspect ratio of 1.32, supporting the interpretation of their subspherical shape (Fig. S7A; SOM1, Table S2). There is an appreciable correlation between their length and width ($r=0.5786$; $R^2=0.7606$; $t(1592)=51.17$, $\rho<0.001$). Although the population is made majority of spherical/subspherical microbodies, few elongated

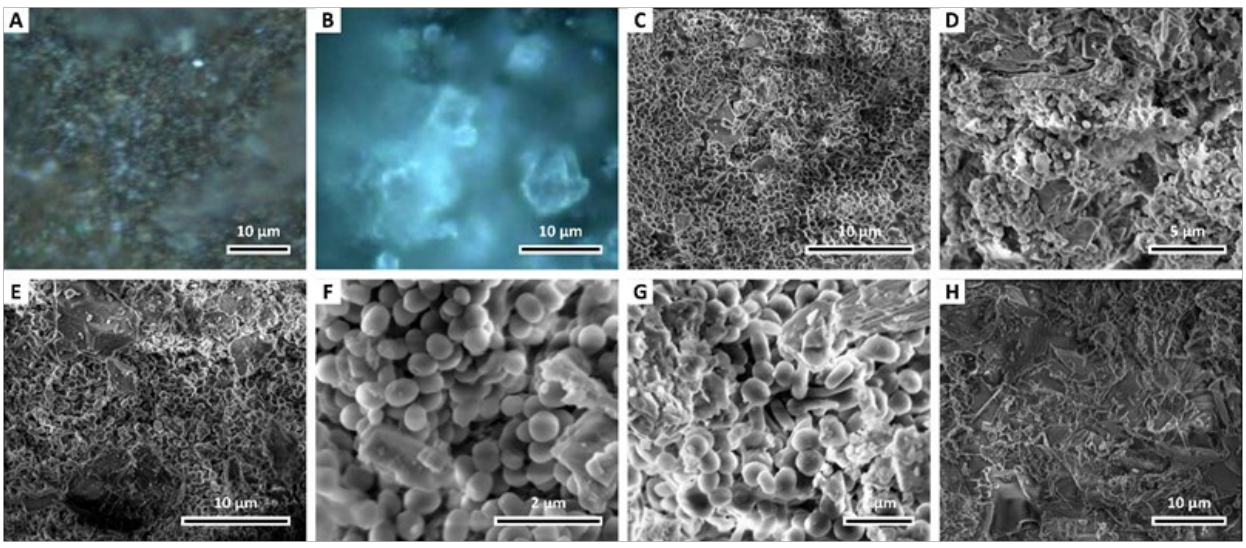

Fig. 3. Confocal optical microscopy and scanning electron microscopy of the fossil fish eye. A, B, COM images of the) the dark brown material in the lower rim of the eye (A), which occurs with a grainy texture, and the host matrix exhibiting the white crystals of calcite (B). C–H, secondary electron (SE) micrograph of a dense population of spherical microbodies observed in the upper (C), centre (D), and lower (E) rims of the eye. F, detail of the microbodies from the eye upper rim, exhibiting a regular subspherical shape with a smooth surface. G, micrograph showing the presence of elongated microbodies among spherical and subspherical granules. H, SE micrograph of the matrix exhibiting the absence of microbodies and presence of crystals.

ones can also be found as seen in Fig. 3G. Thus, considering that two shapes (e.g. spherical and elongated) of microbodies exist, we performed the mixture modelling (MM) analysis of the entire dataset to distinguish these two subpopulations and to compare their proportions. Results indicated that our dataset can be indeed divided into two groups (Figs 4A; SOM1, S7B), but microbodies are essentially spherical/subspherical with 91.71% (n = 132) of total population, whilst elongated consist of only 8.29% (n = 1461). Statistical analysis indicates that Group 1 have moderate correlation values ($r = 0.6335$; $R^2 = 0.7960$, $t(131) = 27.53$, $\rho < 0.001$) whereas Group 2 have strong correlation ($r = 0.8720$; $R^2 = 0.7603$; $t(1460) = 59.51$, $\rho < 0.001$). Dimensionally, the Group 1 consists of elongated microbodies with mean sizes estimated in 0.773 ± 0.229 µm in length, 0.398 ± 0.109 µm in width, and mean AR = 1.95. In turn, the Group 2 is consisted of spherical/subspherical microbodies with average size estimated in 0.619 ± 0.160 µm in length, 0.4967 ± 0.134 µm in width, and mean AR = 1.26 (Fig. 4B; SOM1, Table S2).

The EDS point-and-shoot analysis (Figs 5; SOM1, S2) revealed that, from the 15 elements detected, microbodies exhibited a larger suite (n = 12) with different intensity in comparison with the matrix (n = 10). Nevertheless, both fossil microbodies and matrix crystals are enriched with three similar elements, C, O, and Ca but values appear with different proportions (Fig. 5). Whilst the fossil is comparatively more enriched in C, the matrix is enriched in Ca, however, both regions show a comparable relative intensity of O. Additionally, Fe is limited to the matrix, whereas S is slightly enriched in the fossil microbodies, but Mg levels are similar in both microbodies and matrix. Other elements occur with negligible or trace amounts below the equipment's detection limit (<0.5%). On the other hand, the non-detection of these elements may also reflect their true absence in the sample. This may be the case of Cu and Zn, which are important elements often related to melanin in fossil and extant samples (Wogelius *et al.* 2011; Egerton *et al.* 2015; Edwards *et al.* 2016; Rossi *et al.* 2020, 2021). Because in previous investigations these elements were found in tissues of *Dastilbe* fish (see Osés *et al.* 2017), the absence of both Cu and Zn can be considered authentic. Interestingly, both elements were also not found in the eyes of a fossil crane fly and two fishes from the Eocene Für Formation, Denmark (Lindgren *et al.* 2012, 2015, 2019), nor in the orbital region of an enantiornithine bird from Jehol Biota, China (Tanaka *et al.* 2017). Notwithstanding, a study of the fish larvae from the Eocene Stolleklint Clay (Denmark), detected Cu but not Zn in the eyes (Heingård *et al.* 2021). Therefore, the absence of both Cu and Zn in the eyes of many fossil fishes indicate the transient nature of these elements and their absence in GP/2E-9378b is not accidental.

Raman spectroscopy of the samples (Fig. 6A–D; SOM1, Table S1, Figs S3, S4; SOM2, Tables S1-S4) show that the matrix is composed of calcite with an influence of phosphates (SOM1, Fig. S4). Whilst the fish eye clearly show Raman bands of melanin (Fig. 5A; SOM1, Fig. S3), which are also similar to kerogeneous materials that exhibit the 'D and G bands' of the amorphous carbons. When compared to that of a helmeted guineafowl feather, the spectra of the brown material from the fossil eye are similar to eumelanin composition from natural (*Sepia officinalis*) and synthetic forms. However, spectra from the fossil eye material are nearly indistinguishable to that of synthetic melanin in that both exhibit intense double broad bands around 1370 ± 4 cm^{-1} and 1570 ± 4 cm^{-1}. On the other hand, the guineafowl brown feather and *Sepia* melanin not only exhibit these doublets, but they also show an additional band at around 1199 cm^{-1} or 1205 cm^{-1}, respectively. Raman Spectroscopy map of the eye support the single point spectra, indicating a spatial correlation of CO_3 band and D & G bands (Fig. 5B-D). The deconvolution of these broad doublet bands in the fossil spectra resulted in five additional (D1-D5 and G bands) in the range of 1000-1800 cm^{-1}. While the 'D-band' vary both red- and blueshift range-directions, the 'G-bands' only appear to change in the redshift side (SOM1: Fig. S5; SOM2, Table S1-S4).

The spectrum of the host rock indicates that diagnosable bands are limited to the fingerprint region of the spectra, ca. 200-2000 cm^{-1} (Smith & Dent 2005). Both matrix and the mid-eye show bands centred at about 290-292 cm^{-1}, 719-720 cm^{-1}, 968-981 cm^{-1}, and 1094-1095 cm^{-1} (SOM2, Table S1-S4). These bands are consistent with vibration modes of carbonates ν_1 and $\nu_4(CO_3)$, and phosphates $\nu_1(PO_4)$, which may be occurring as calcite in the matrix, and/or hydroxyapatite from small fragments of bones or phosphatized tissues (Gunasekaran *et al.* 2006; Gunasekaran & Anbalagan 2008; Buzgar & Apopei 2009; Morris & Mandair 2011). Additionally, it is also possible to observe a very weak band at ca. 515 cm^{-1} in one spectrum which most likely is the $\nu_2(PO_4)$ from diagenetically altered hydroxyapatite (Marques *et al.* 2018). No Raman bands of calcite were observed in the fish eye containing the microbodies.

The FTIR data further support the Raman Spectroscopy results (Fig. 6 E-I; SOM1, Fig. S6; SOM2, Table S5), with the presence of stretching bands of hydroxyls (3700-3100 cm^{-1}), C–H (ca. 3050-2850 cm^{-1}), carbonates (ca. 2650-2450 cm^{-1}), carbonyls (ca. 1850-1500 cm^{-1}), amide III (1200-1350 cm^{-1}), C–O (ca. 1200-1100 cm^{-1}), phosphates (ca. 900-800

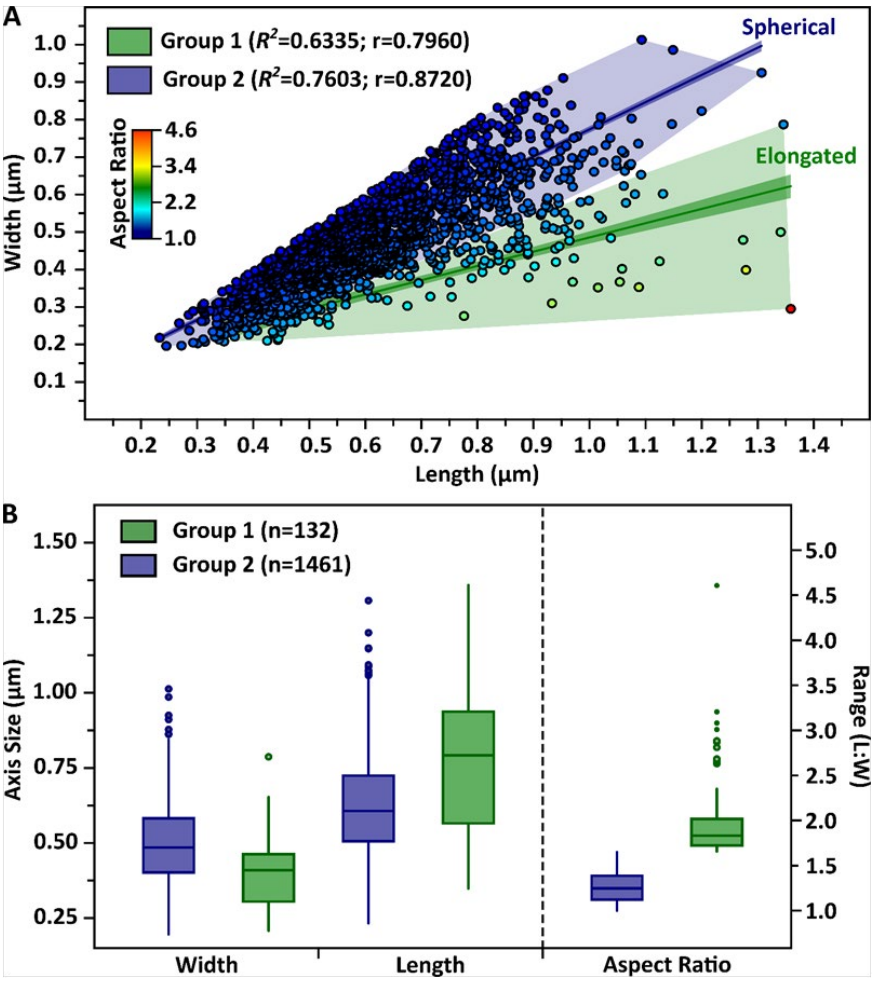

Fig. 4. Statistical analysis of the microbodies. A, scattered plot of the microbodies (n=1593) indicating the relationship between the axis (length vs width), and their correlation/determination values. This image also shows that two subpopulations (i.e., groups) can be identified through the mixture analysis, with elongated (n=1461) and spherical microbodies (n=132). B, boxplot chart showing the range of sizes and aspect ratio of each group.

cm^{-1}), and bending of methyl (ca. 1500-1400 cm^{-1}) (Gunasekaran *et al.* 2006; Movasaghi *et al.* 2008; Perna *et al.* 2016; Monnier *et al.* 2018; So *et al.* 2020). Furthermore, the amide III band is consisted of at least three others bands, such as, C–N, C–C, and C–OH from stretching of pyrroles, indole rings and phenolic group (SOM2, Table S5). In addition, the molecular mapping indicates the spatial distribution of some functional groups, especially the bands of O–H that occur mainly in the fossil and the bone.

Finally, although the use of geothermometer is not directly indicated for the study of maturation of organic carbons in low grade metamorphic rocks, we decided to apply it to test if the alteration temperature for the eumelanin could be retrieved since this pigment generally is transformed into kerogen-type compound in the geological record. Results, suggest metamorphic zones between diagenesis and catagenesis. It is important to note that it is uncertain if a geomacromolecule derived from a likely more homogeneous organic material, such as the biopolymer melanin inside melanosomes, would be comparable to data derived from the more typical kerogen types or macerals used in previous studies. Nevertheless, the values reported here are broadly similar to the ones reported by Goldberg *et al.* (2017) for the Santana Group, which range from 0.29-0.6%.

Discussion

Considering the morphological and chemical evidence, the observed microbodies in GP/2E-9378b can be confidently identified as fossilised

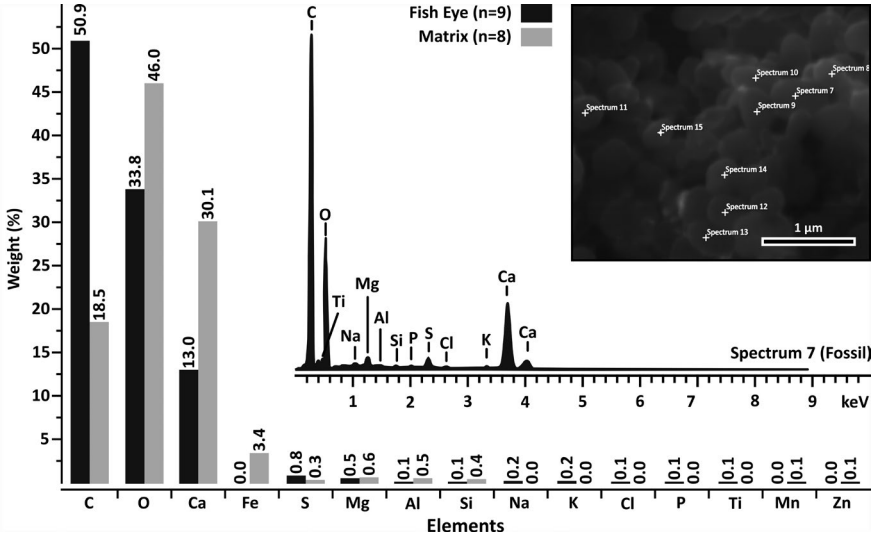

Fig. 5. EDS point-and-shoot analysis. Bar chart summarizing the mean values of all spots, showing the relative intensity from both eye microbodies (soft tissue) and host matrix. Inset: the spectrum from the microbodies seen in the micrograph.

eumelanin-bearing melanosomes (Roy *et al.* 2020b). These results are consistent with the presence of pigments in life (Dubey & Roulin 2014), and due to the limited distribution of the fossil melanin residues to the eye tissue, they are likely not a consequence of displaced internal or integumentary melanosomes (McNamara *et al.* 2018).

The Raman bands observed in the fossil and guineafowl feather exhibit remarkable similarity with those seen in modern melanin samples, whilst the matrix shows bands of calcite. Together with the occurrence and morphology of the carbon-rich microbodies, the results from the vibrational spectroscopy (RS and FTIR) allow us to attribute these spectra to fossilized melanin, i.e. geomelanin. Furthermore, the positions of the Raman and FTIR bands are consistent to those seen in the literature for extant (Perna *et al.* 2016; and references therein) and fossil eumelanin (Košťák *et al.* 2018; Gaspard *et al.* 2019; Pinheiro *et al.* 2019; Rossi *et al.* 2022). These bands can be assigned to various vibrational modes of the pyrrole, indole units, amines, and its functional groups (Capozzi *et al.* 2005; Centeno & Shamir 2008; Kim *et al.* 2013; Perna & Capozzi 2012; Perna *et al.* 2013, 2016). For instance, the first Raman band, between 1300 cm^{-1} to 1400 cm^{-1}, likely represents an overlap of many vibrational modes, such as the stretching of C=N and C—N bonds from pyrrole rings, combined with in-plane deformation of C=C and C=N of both pyrrole and indole moieties. The second band, between 1500 cm^{-1} to 1600 cm^{-1}, can be assigned to stretching vibration of C=C from aromatic rings. The third band generally occurs between 1100 cm^{-1} to 1250 cm^{-1}, and most likely represent C—O stretching or O—H in-plane deformation of carboxylic acid (Capozzi *et al.* 2005; Centeno & Shamir 2008; Perna & Capozzi 2012; Perna *et al.* 2013, 2016).

Albeit recent studies suggested that it is possible to distinguish geomelanin from carbonaceous compounds from other sources (Rossi *et al.* 2024; Li *et al.* 2024), the experimental setup used far simulate the real conditions of melanin degradation and the chemical dynamics that usually leads to the formation of kerogen. In contrast, degradation of melanized tissues in sediment encased experiments indicate a nearly undistinguishable spectra with kerogen (GP, unpublished data 2024). Therefore, because melanin usually is diagenetically altered, through the loss of volatile components and extensive polymerization/crosslinking, is not wrong considering that this pigment can be transformed into a more kerogen-type substance over long time (Muscente *et al.* 2018; Roy *et al.* 2023). In this scenario, although the analysis of the eye indicates that the spectra are similar to eumelanin, they also resemble the characteristic 'D and G bands' of disordered and graphitic kerogen (Huang *et a*l. 2004), and here, these doublet bands can also be referred here as the 'D and G bands of geomelanin'. Moreover, in the *Dastilbe* case, the organic matter derived from melanin could also be crosslinked to some extent to other byproducts of tissue decay from the eye and other body parts, including those highly pigmented. Indeed, the broadness of these double bands likely indicates the influence of several vibration modes of a complex macromolecule that is akin to the disordered

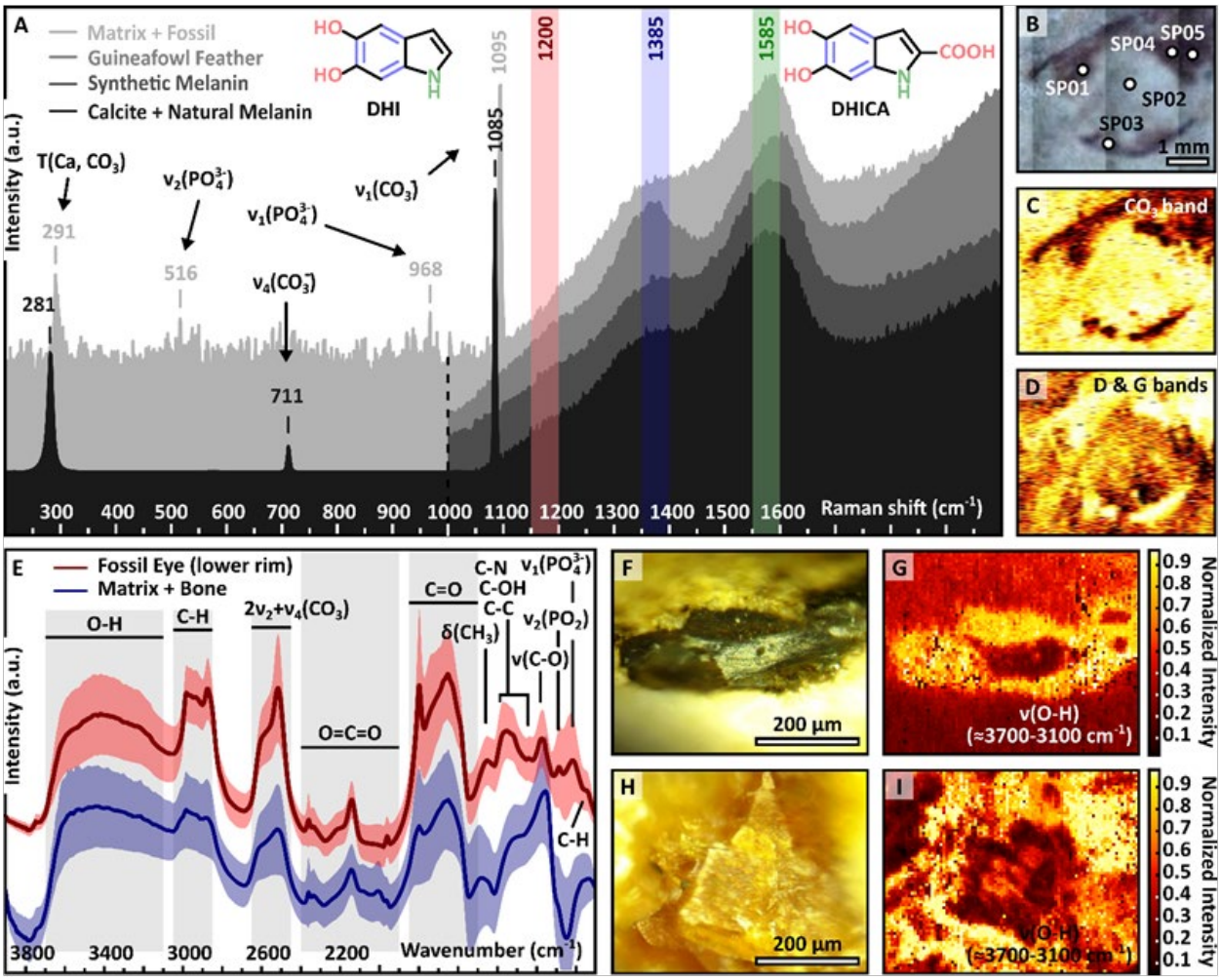

Fig. 6. Vibrational spectroscopy of the GP/2E-9378b and extant samples. A, spectra at the fingerprint region taken from the matrix and standard calcite mineral and band assignments. Image (A) also shows spectra from the fossil eye, the guineafowl feather, DHI-rich synthetic melanin, and DHICA-rich natural melanin (with molecular structure of the monomers of each type), above the 1000 cm^{-1} (dashed line). Standard bands and molecular bonding of melanin are show as vertical number and coloured lines. B, optical image of the region mapped from where the five point-and-shoot spots analysis were made. C, map from the 1070 to 1100 cm^{-1} range which corresponds to the $\nu_1(CO_3)$. D, map from the D and G band range, between 1100-1700 cm^{-1}. E, spectra from the previous maps from the fossil eye, matrix + bone; showing bands of the organic matter, phosphates, and carbonate. F, H, optical image of the upper rim of the eye and matrix where the FTIR spatial map was performed. G, I, FTIR map from the F and H figures at the 3700 to 3100 cm^{-1} range that correspond to the ν(O−H). For detailed assignments, see SOM2, Table S5.

and heterogeneous nature of eumelanin and an amorphous carbonaceous matter (Huang *et al.* 2004).

The production of synthetic melanin results in a compound rich in, if not solely consisting of, DHI precursors (Costa *et al.* 2012). In contrast, both moieties are present in natural melanin, although DHICA generally predominates (Roldán *et al.* 2014). Here, we observed that the Helmeted Guineafowl spectra are strikingly similar to that of *Sepia* melanin, whereas the fossil fish eye is unexpectedly more similar to that of the synthetic melanin. Consequently, it is possible that many, if not most, carboxylates in the fossil fish melanin were lost during diagenesis, resulting in an enrichment of DHI. It has been already shown that during melanin thermal maturation, DHICA monomers lose their carboxylates, promoting extensive crosslinking between moieties besides being bonded with environmental metals and other surrounding polymers (Ito *et al.* 2013). Notably, experiments have shown that Ca^{2+} and Mg^{2+} generally bind with the $RCOO^-$ and OH sites of the eumelanin structure (Hong & Simon 2007). In this case, the fossil fish geomelanin might be enriched with calcium, in addition to minor amounts of sulphur and magnesium.

Because the DHICA of this fossil eye appears to have partially lost their carboxylates, we hypothesize that these metals and other compounds – even melanin monomers and moieties – possibly tended to bind at this site. It is also possible that diagenesis exposed the DHI moieties to dehydration, inducing loss of OH and allowing organics and metals to bind at the vacant sites (Fig. 7A). The Raman spectroscopy data seem to support this, since the band related to the carboxylic acid and hydroxyls (around 1200-1250 cm^{-1}) disappear or decreases in the geomelanin spectra (Fig. 7B). This interpretation is further supported by other studies of fossil melanosomes as well as in maturation experiments (Pinheiro *et al.* 2019; Rossi *et al.* 2020, 2021). Furthermore, it might be the case that the occupation of these sites by the metals possibly contributed to the molecular stability of the geomelanin, increasing its chemical resistance to further diagenetic changes; however, this hypothesized effect still needs to be observed experimentally.

Despite that the host rock minerals may have contributed to the spectra, the presence of the Ca in the fossil eye may be also explained by *in vivo* and/or post-mortem accumulation/adsorption during life through exposure to calcium-rich waters. Furthermore, at least in part, incorporation could be further compounded when the saturation of Ca ions around the decaying carcass reached their highest level. Since we did not find bands related to calcite in the melanosome-rich regions, it is also plausible that some Ca ions could have been incorporated into the melanin oligomers during mesodiagenesis, where Ca became available through the dissolution/recrystallization of authigenic calcite crystals. This process was likely responsible for releasing a significant concentration of Ca, which likely led to some Ca incorporation into the eumelanin monomers. Moreover, according to our estimation of the melanin thermal alteration, based on the fact that geomelanins can also be converted into kerogen-type macromolecules, the Raman parameters (mainly G-FWHM) suggest a thermal maturity similar to vitrinite reflectance (VR_o) values ranging from ca. 0.3% to ca. 1.5-2% in accordance with recent compiled trends (see Henry *et al.* 2019; Schito *et al.* 2023). These results point to an immature to mature kerogen, broadly in agreement with VR_o values reported by Goldberg *et al.* (2017), which suggested immature to only marginally mature organic matter for the Santana Group (see SOM2, Table S6). All together, these data are also consistent with studies of palaeotemperature in the Araripe Basin, which suggested that the temperature did not exceed the 110 °C during basin evolution (Morais Neto *et al.* 2006).

Supposed cones and rods have been reported preserved in exceptional fossils in the Carboniferous fish of Mazon Creek of USA and putatively in a Cretaceous dinosaur from Jehol Biota of China (Tanaka *et al.* 2014, 2017). However, both types of photoreceptors are missing in GP/2E-9378b. This absence is, perhaps, to be expected because these cells are very delicate and similar to other cellular tissues, i.e. they are prone to be lost early in decay. This is particularly especial to *Dastilbe* fish whose preservation favoured other more recalcitrant tissues, such as muscle fibres (Osés *et al.* 2017). Nevertheless, this fossil exhibits an abundance of spherical to subspherical microbodies, indicating that melanin permitted the preservation of the pigmented layers of the eye, such as the *tapetum lucidum* of the retinal pigmented epithelium (RPE). Nevertheless, this explanation may be biased, since it is possible that most eye remnants remained on the now lost counterpart. Anyhow, if we reject this interpretation, then the low abundance of elongated melanosomes is puzzling, given the wide range of melanosome shapes in extant eyes that varies from elongated to oval forms. As a result, it is possible that both morphologies were present in the retina *in vivo*, such as the seen in many fossil organisms, such as putative early cyclostomes (Clements *et al.* 2016; Gabbott *et al.* 2016; Rogers *et al.* 2019; Gabbott *et al.* 2021), teleost fishes (Lindgren *et al.* 2012; Tanaka *et al.* 2014; Lindgren *et al.* 2015; Heingård *et al.* 2021; Rossi *et al.* 2022), aquatic reptiles (Lindgren *et al.* 2010, 2018), and dinosaurs (Vinther *et al.* 2008; Tanaka *et al.* 2017). On the other hand, although unlikely, it is also possible that the oblate melanosomes in GP/2E-9378b possibly had - counterintuitively - a different melanin composition (i.e. being greater phaeomelanin concentration). Since phaeomelanins are less stable than other melanins (Vinther 2020), during fossilization the loss of this pigment would favour the concentration of eumelanin creating an artificial biased concentration of this polymer. Indeed, this may be the case of the pterosaur *Tupandactylus imperator* from the Crato Formation, in which only subspherical microbodies were detected in many parts of the headcrest (Pinheiro *et al.* 2019). Alternatively, it is possible that most elongated melanosomes were removed when the matrix was split open, but this explanation would require the admission that a select removal of these microbodies occurred naturally. In another scenario, it is also possible that this eye had originally only a meagre quantity of these elongated melanosomes. Conspicuously, this pattern of distribution is consistent with the hypothesis that microbody abundance decreases from the eye's border to the centre (Durairaj *et al.* 2012; Burgoyne *et al.* 2015).

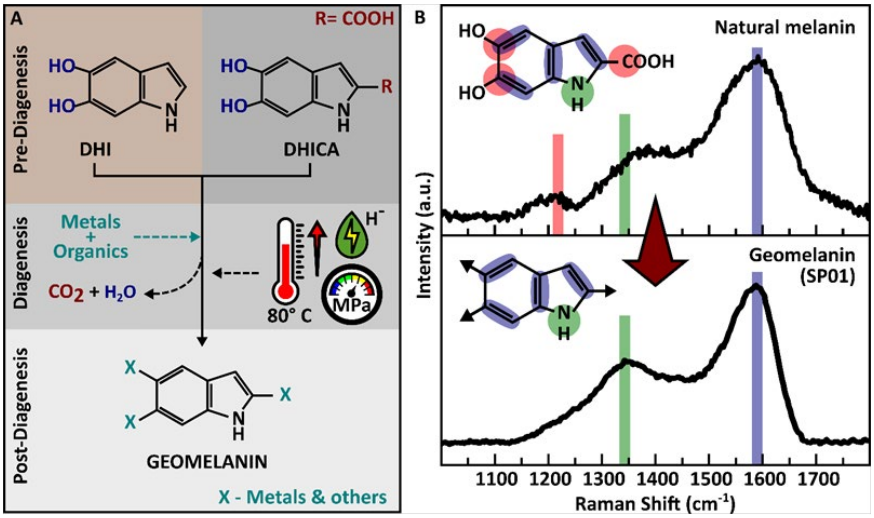

Fig. 7. Formation of geomelanin. A, the possible pathway suggested by the Raman spectroscopy in which the DHICA and DHI units are converted into a melanin enriched with DHI-like moieties. In this proposal, the DHICA and DHI moieties lose their RCOOH and phenolic OH during diagenesis with increase of temperature and pressure, additionally with the influence of acidic pH. This leads to the formation of DHI derivative with vacant sites that would be occupied with metals and organics (e.g. polymers). B, spectra of natural (*Sepia* melanin) and diagenetically altered geomelanin (seen in spectrum SP01 of the fossil eye), indicating that spectra may be able to reflect its preservation, with changes in molecular composition (loss of COOH and OH).

Despite these hypotheses, around 92% of all melanosomes of GP/2E-9378b eye is consisted of spherical/subspherical microbodies, and their presence is limited to the eye rims (i.e. the dark organic stains). This interpretation would be in agreement with the fact that in modern eyes, the abundance of spherical melanosome increases towards the periphery (distal part, the region preserved in our specimen), but at the same time, decreases with age (Schmidt & Peisch 1986). Indeed, the low frequency of elongated melanosomes could be explained by their location in the preserved tissue, as most of elongated melanosomes are located, and somewhat oriented, in the distal part of the of RPE (Vinther *et al.* 2008; Lindgren *et al.* 2012; Clements *et al.* 2016). A similar predominance of sub-spherical melanosomes was observed in the eyes of the elasmobranch *Bandringa* from the Carboniferous Mazon Creek *Lagerstätte* (Clements *et al.* 2016). Therefore, assuming that the pattern is not taphonomically driven, and considering the disparate abundance of spherical/subspherical microbodies, this result may indicate that, at least in this fish taxa, melanosome shape may have been not diverse as seen in other species. In any case, this phenomenon still needs to be verified whether with better preserved and/or numerous specimens.

Considering that modern fish eyes are not that different from their Silurian ancestors (and extant descendants) whose eye were already well developed (Land 2014), it is possible that similar visual acuity was present in extinct fish lineages from the Cretaceous; and this may be the case of the *Dastilbe* fish. The sole living relative of *Dastilbe*, the milkfish (*Chanos chanos* Forsskål, 1775), are sensitive to blue-green and orange-red wavelengths, and hence, able to see in colour (Kawamura & Nishimura 1980). However, the specimen studied exhibited some particularities that mostly are derived from taphonomy, such as the lack (degradation) of preserved photoreceptors and remarkable low abundance of elongated melanosomes. Notwithstanding, these characteristics are remarkably different to another report, in which no structure other than calcite crystals from the surrounding matrix was found in the ocular region, suggesting that most tissues were lost during decay and diagenesis (Osés *et al.* 2017).

In most fish eyes, image focusing is only obtained when their spherical lenses are moved forward to or backward from the eye surface. Due to this, fish can see a maximum distance up to 20 m, but generally, their vision is limited to one metre (Glaeser & Paulus 2015). Conspicuously, juvenile individuals of the milkfish have hyperopic vision (Chang *et al.* 2009a), and assuming that *D. crandalli* may have had a similar visual trait, it is possible to suggest that this fish was also hyperopic. Similar to milkfish, this farsightedness may also be related to the environment that this fish inhabited (Bagarinao 1991). In the transition between larvae to juvenile stage, the milkfish also change their habitat and, consequently, their visual

acuity (Chang *et al.* 2009b). This shift to the sea shallow waters, which have clearer waters compared to the coastal and near-shore settings, favours the development of the young milkfish eyes to better receive short wavelengths (violet-blue hues), typical of the open sea (Chang *et al.* 2009b). If we assume that *Dastilbe* had a similar visual capability as its kin, it is possible that this fish also dwelled in the shallow and brackish waters of the Crato palaeolake (Warren *et a*l. 2017). Since these shallower portions were teeming with life both inside and outside the body of water – as seen by the abundant record of fossil small animals – this visual capacity may have also impacted the *Dastilbe's* survival. It was in these regions that these fish could feed on the abundant plankton and smaller animals, such as cyanobacteria, ostracods, insects, larvae (Mendes *et al.* 2023), and even smaller *Dastilbe* specimens (Salgado & Carvalho 2023).

Despite all that, it is important to recognize that the presence of retinal melanin alone can be associated with the capacity to discern light from shade. Also, highly pigmented eyes are usually associated with animals that are active at night or live in dim light (Nicol *et al.* 1973; Land & Nilsson 2012). The presence of oblate microbodies, in some way, is also consistent with the hypothesis that melanin significantly contributes to visual acuity aside colour perception. In the case of GP/2E-9378b, assuming that taphonomic biases are not at play, it is possible to suggest that the visual capability of *Dastilbe* was limited compared to other fish specimens. In other words, the low diversity but the high density of melanosomes from RPE would imply that this fish was at least adapted to discern light from shade in shorter distances, and hence, being adapted to live in low light environment, such as in turbid or shaded waters by aquatic plants (Ribeiro *et al.* 2021; Gobo *et al.* 2023) of the palaeolake. Nevertheless, we recognize that further investigations on exceptionally preserved individuals or with larger number of specimens would provide evidence to support this study.

Conclusions

Assuming that taphonomic bias is not at play, the evidence presented in this paper indicates that the examined *Dastilbe crandalli* fish exhibit low diversity of melanosome shape, with spherical to subspherical representing 91% of the total. This result also indicates that this fish had a limited visual capability compared to extant fishes, but at the same time, they may have been adapted to shadowing portions of the palaeolake. We also noted that the estimated temperature of alteration of geomelanin is consistent to the diagenesis of the Crato beds, with relatively little volatilization and polymerization/crosslinking compared to other fossil melanin. Furthermore, this result also indicates that geothermomether can be successfully applied to infer the level of maturation of the geomelanin. Since melanosomes and melanin is an important trait in the biology of fish, we hope that new investigations on this subject, and in a greater number of specimens, will give new information about the palaeoecology of this, as well as others, largely overlooked fish.

Acknowledgements.– We acknowledge Lorian C. Straker (CENABIO-UFRJ), and Evelyn A. M. S. Bizan (UFVJM) for fruitful discussions and suggestions that improved the earlier drafts of the manuscript. We are indebted to Luiz Fernando Kilesse Salgado (UFRJ) and Rafael M. Lindoso (IFMA) for help in identifying the specimen. We thank Fabiano Montoro, João Marcos da Silva, and Élcio L. Pires (LNNano CNPEM), for their invaluable support on the SEM-EDS analysis at the LNNano and Mírian L. A. F. Pacheco (UFSCar), Paula A. Sucerquia (UFPE), and Thomas R. Fairchild (IGc-USP) for helpful discussions. We are indebted to Juliana L. Moraes and Ivone C. Cardozo (IGc-USP) for their support, and for providing access to the fossil and equipment used herein. We also thank the postdoctoral programs of the Institute of Chemistry, Institute of Geosciences, and Institute of Physics from the University of São Paulo. We also thank the Collaborating Researcher Program of the Institute of Physics from the University of São Paulo. This research used facilities of the Brazilian Nanotechnology National Laboratory (LNNano), part of the Brazilian Centre for Research in Energy and Materials (CNPEM), a private non-profit organization under the supervision of the Brazilian Ministry for Science, Technology, and Innovations (MCTI). The LNNano staff are acknowledged for the assistance during the experiment, proposal SEM-23696. This study was financed in part by the National Council for Scientific and Technological Development (CNPq 142246/2019-0) and the Sandwich Doctorate scholarship from Coordination for the Improvement of Higher Education Personnel (CAPES-PRINT 88887.466483/2019-00) both awarded to GP. It also had the support of Carlos Chagas Filho Foundation for Research Support in the State of Rio de Janeiro (FAPERJ E-26/200.828/2021 E-26/200.998/2024) and (CNPq 303596/2016-3) to ISC; and the São Paulo Research Foundation (FAPESP) for the postdoctoral grants: 2020/11320-0 and 2022/06133-1 to BBK, 2021/07007-7, 2022/06485-5, and 2023/14250-0 to GLO, and 2023/10680-0 to GP. The FAPESP is also acknowledged for the grant number 2021/05083-8 to DG support on the Raman Spectrometer grant (2012/18936-0).

Supplementary material

File SOM1: Supplementary Text, Figures (S01-S07) and Tables (S1 and S2).
File SOM2: Tables (S1–S6)

References

Agius, C. & Roberts, R.J. 2003: Melano macrophage centres – and their role in fish pathology: *Journal of Fish Diseases 26*, 499-509. https://doi.org/10.1046/j.1365-2761.2003.00485.x

Asari, M.W. & Nadeem, A. 2016: *Atlas of Ocular Anatomy*. Springer, Cham.

Arai, M. & Assine, M.L. 2020: Chronostratigraphic constraints and paleoenvironmental interpretation of the Romualdo Formation (Santana Group, Araripe Basin, Northeastern Brazil) based on palynology. *Cretaceous Research 116*, 104610. https://doi.org/10.1016/j.cretres.2020.104610

Assine, M.L., Perinotto, J.A.J., Custódio, M.A., Neumann, V.H., Varejão, F.G. & Mescolotti, P.C. 2014: Sequências deposicionais do Andar Alagoas da Bacia do Araripe, Nordeste do Brasil. *Boletim de Geociências da Petrobrás 22*, 3–28.

Bagarinao, T.U. 1991: *Biology of Milkfish (*Chanos chanos *Forsskål)*. Aquaculture Department of the Southeast Asian Fisheries Development Center, Tigbauan.

Bellono, N.W. & Oancea, E.V. 2014: Ion transport in pigmentation. *Archives of Biochemistry and Biophysics 563*, 35–41. https://doi.org/10.1016/j.abb.2014.06.020

Bernardes-de-Oliveira, M.E.C., Sucerquia, P.A., Mohr, B., Dino, R., Antoniolli, L. & Garcia, M.J. 2014: Indicadores paleoclimáticos na paleoflora do Crato, final do Aptiano do Gondwana Norocidental. In: Carvalho, I.S., Garcia, M.J., Lana, C.C., Strohschoen, O., Jr. (eds). Paleontologia: Cenários de Vida - Paleoclima. Rio de Janeiro, Brazil. *Interciência 5*, 99-118.

Bonser, R.H.C. & Witter, M.S. 1993: Indentation hardness of the bill keratin of the European starling. *The Condor 95*, 736-738. https://doi.org/10.2307/1369622

Bonser, R.H. 1995: Melanin and the abrasion resistance of feathers. *The Condor 97*, 590-590. https://doi.org/10.2307/1369048

Borovanský, J. & Riley, P.A. 2011: *Melanin and Melanosomes: Biosynthesis, Biogenesis, Physiological, and Pathological Functions*. Wiley-Blackwell, New York. https://doi.org/10.1002/9783527636150

Briggs, D.E.G. & Summons, R.E. 2014: Ancient biomolecules: Their origins, fossilization, and role in revealing the history of life. *BioEssays 36*, 482–490. https://doi.org/10.1002/bies.201400010

Burgoyne, T., O'Connor, M.N., Seabra, M.C., Cutler, D.F. & Futter, C.E. 2015: Regulation of melanosome number, shape and movement in the zebrafish retinal pigment epithelium by OA1 and PMEL. *Journal of Cell Science 128*, 1400-1408. https://doi.org/10.1242/jcs.164400

Buzgar, N. & Apopei, A.I. 2009: The Raman study of certain carbonates. *Analele Stiintifice Universitatii, Al. I. Cuza Iasi Geologie 55*, 97-112.

Campos, A.P.C., Carvalho, R.T. de, Straker, L.C., Salgado, L.T., Kellner, A. & Farina, M. 2019: Combined microscopy and spectroscopy techniques to characterize a fossilized feather with minimal damage to the specimen. *Micron 120*, 17–24. https://doi.org/10.1016/j.micron.2019.01.016

Capozzi, V., Perna, G., Gallone, A., Biagi, P.F., Carmone, P., Fratello, A., Guida, G., Zanna, P. & Cicero, R. 2005: Raman and optical spectroscopy of eumelanin films. *Journal of Molecular Structure 744-747*, 717-721. https://doi.org/10.1016/j.molstruc.2004.11.074

Carvalho, I.S., Novas, F.E., Agnolín, F.L., Isasi, M.P., Freitas, F.I. & Andrade, J.A. 2015: A Mesozoic bird from Gondwana preserving feathers. *Nature Communications 61*, 1-5. https://doi.org/10.1038/ncomms8141

Catto, B., Jahnert, R.J., Warren, L.V., Varejão, F.G. & Assine, M.L. 2016: The microbial nature of laminated limestones: Lessons from the Upper Aptian, Araripe Basin, Brazil. *Sedimentary Geology 341*, 304–315. https://doi.org/10.1016/j.sedgeo.2016.05.007

Centeno, S.A. & Shamir, J. 2008: Surface enhanced Raman scattering (SERS) and FTIR characterization of the *Sepia* melanin pigment used in works of art. *Journal of Molecular Structure 873*, 149-159. https://doi.org/10.1016/j.molstruc.2007.03.026

Chang, C.-H., Chiao, C.-C. & Yan, H.Y. 2009a: The structure and possible functions of the milkfish *Chanos chanos* adipose eyelid. *Journal of Fish Biology 75*, 87-99. https://doi.org/10.1111/j.1095-8649.02266.x

Chang, C.-H., Chiao, C.-C. & Yan, H.Y. 2009b: Ontogenetic changes in color vision in the milkfish (*Chanos chanos* Forsskål 1775). *Zoological Science 26*, 349-355. https://doi.org/10.2108/zsj.26.349

Cincotta, A., Nicolai, M., Nascimento-Campos, H.B., McNamara, M. D'Alba, L., Shawkey, M.D., Kischlat, E.-E., Yans, J., Carleer, R., Escuillié, F. & Godefroit, P. 2022: Pterosaur melanosomes support signaling functiong for early feathers. *Nature 604*, 684-688. https://doi.org/10.1038/s41586-022-04622-3

Clements, T., Dolocan, A., Martin, P., Purnell, M.A., Vinther, J. & Gabbott, S.E. 2016: The eyes of *Tullimonstrum* reveal a vertebrate affinity. *Nature 53*2, 500–503. https://doi.org/10.1038/nature17647

Coimbra, J.C. & Freire, T.M. 2021: Age of the post-rift sequence I from the Araripe Basin, Lower Cretaceous, NE Brazil: Implications for spatio-temporal correlation. *Revista Brasileira de Paleontologia 24*, 37–46, https://doi.org/10.4072/rbp.2021.1.03

Coimbra, J.C., Arai, M. & Carreño, A.L. 2002: Biostratigraphy of Lower Cretaceous microfossils from the Araripe Basin, northeastern Brazil. *Geobios 35*, 687–698. https://doi.org/10.1016/S0016-6995(02)00082-7

Colleary, C., Dolocan, A., Gardner, J., Singh, S., Wuttke, M., Rabenstein, R., Habersetzer, J., Schaal, S., Feseha, M., Clemens, M., Jacobs, B.F., Currano, E.D., Jacobs, L.L., Sylvestersen, R.L., Gabbott, S.E. & Vinther, J. 2015: Chemical, experimental, and morphological evidence for diagenetically altered melanin in exceptionally preserved fossils. *Proceedings of the National Academy of Sciences 112*, 12592–12597. https://doi.org/10.1073/pnas.1509831112

Costa, T.G., Younger, R., Poe, C., Farmer, P.J. & Szpoganicz, B. 2012: Studies on synthetic and natural melanin and its affinity for Fe(III) ion. *Bioinorganic Chemistry and Applications 712840*, 1-9. https://doi.org/10.1155/2012/712840

Cuthill, I.C., Allen, W.L., Arbuckle, K., Caspers, B., Chaplin, G., Hauber, M.E., Hill, G.E., Jablonski, N.G., Jiggins, C.D., Kelber, A., Mappes, J., Marshall, J., Merrill, R., Osorio, D., Prum, R., Roberts, N.W., Roulin, A., Rowland, H.M., Sherratt, T.N., Skelhorn, J., Speed, M.P., Stevens, M., Stoddard, M.C., Struart-Fox, D., Talas, L., Tibbetts, E. & Caro, T. 2017: The biology of color. *Science 357*, eaan0221. https://doi.org/10.1126/science.aan0221

D'Alba, L. & Shawkey, M.D. 2019: Melanosomes: Biogenesis, properties, and evolution of an ancient organelle. *Physiological Reviews 99*, 1-19. https://doi.org/10.1152/physrev.00059.2017

Dias, J.J. & Carvalho, I.S. 2020: Remarkable fossil crickets preservation from Crato Formation (Aptian, Araripe Basin), a Lagerstätten from Brazil. *Journal of South America Earth Sciences 98*, 102443. https://doi.org/10.1016/j.jsames.2019.102443

Dias, J.J. & Carvalho, I.S. 2022: The role of microbial mats in the exquisite preservation of Aptian insect fossils from the Crato Lagerstätte. Brazil. *Cretaceous Research 130*, 105068. https://doi.org/10.1016/j.cretres.2021.105068

Dias, J.J., Carvalho, I.S., Buscalioni, A.D., Umamaheswaran, R., López-Archilla, A.I., Prado, G. & Andrade, J.A.F.G. 2023: Mayfly larvae preservation from the Early Cretaceous of Brazilian Gondwana: Analogies with modern mats and other Lagerstätten. *Gondwana Research 124*, 188–205. https://doi.org/10.1016/j.gr.2023.07.007

D'Ischia, M., Wakamatsu, K., Napolitano, A., Briganti, S., Garcia-Boron, José-Garcia, Kovacs, D., Meredith, P., Pezzella, A., Picardo, M., Sarna, T., Simon, J.D. & Ito, S. 2013: Melanins and melanogenesis: methods, standards, protocols. *Pigment Cell and Melanoma Research 26*, 616-33. https://doi.org/10.1111/pcmr.12121

Davis, S.P. & Martill, D.M. 1999: The gonorynchiform fish *Dastilbe* from the Lower Cretaceous of Brazil. *Palaeontology 42*, 715-740. https://doi.org/10.1111/1475-4983.00094

Davis, A.L., Thomas, K.N., Goetz, F.E., Robinson, B.H., Johnsen, S. & Osborn, K.J. 2020: Ultra-black camouflage in deep-sea fishes. *Current Biology 30*, 3470–3476. https://doi.org/10.1016/j.cub.2020.06.044

Dubey, S. & Roulin, A. 2014: Evolutionary and biomedical consequences of internal melanins. *Pigment Cell & Melanoma Research 27*, 327-338. https://doi.org/10.1111/pcmr.12231

Durairaj, C., Chastain, J.E. & Kompella, U.B. 2012: Intraocular distribution of melanin in human, monkey, rabbit, minipig and dog eyes. *Experimental Eye Research 98*, 23-27. https://doi.org/10.1016/j.exer.2012.03.004

Edwards, N.P., van Veelen, A., Anné, J., Manning, P.L., Bergmann, U., Sellers, W.I., Egerton, V.M., Sokaras, D., Alonso-Mori, R., Wakamatsu, K., Ito, S. & Wogelius, R.A. 2016: Elemental characterisation of melanin in feathers via synchrotron X-ray imaging and absorption spectroscopy. *Scientific Reports 6*, 34002. https://doi.org/10.1038/srep34002

Egerton, V.M., Wogelius, R.A., Norell, M.A., Edwards, N.P., Sellers, W.I., Bergmann, U., Sokaras, D., Alonso-Mori, R., Ignatyev, K., van Veelen, A., Anné, J., van Dongen, B., Knoll, F. & Manning, P.L. 2015: The mapping and differentiation of biological and environmental elemental signatures in the fossil remains of a 50-million-year-old bird. *Journal of Analytical Atomic Spectrometry 30*, 627-634. https://doi.org/10.1039/c4ja00395k

Freddo, T.F. & Chaum, E. 2018. *Anatomy of the Eye and Orbit: The Clinical Essentials*. Wolters Kluwer, Philadelphia.

Gäb, F., Ballhaus, C., Stinnesbeck, E., Kral, A.G., Janssen, K. & Bierbaum, G. 2020: Experimental taphonomy of fish-role of elevated pressure, salinity and pH. *Scientific Reports 10*, 7839. https://doi.org/10.1038/s41598-020-64651-8

Gabbott, S.E., Donoghue, P.C.J., Sansom, R.S., Vinther, J., Dolocan, A. & Purnell, M.A. 2016: Pigmented anatomy in Carboniferous cyclostomes and the evolution of the vertebrate eye. *Proceedings of the Royal Society B 283*, 20161151. https://doi.org/10.1098/rspb.2016.1151

Gabbott, S.E., Sansom, R.S. & Purnell, M.A. 2021: Systematic analysis of exceptionally preserved fossils: correlated patterns of decay and preservation. *Palaeontology 64*, 789-803. https://doi.org/10.1111/pala.12571

Gaspard, D., Paris, C., Loubry, P. & Luquet, G. 2019: Raman investigation of the pigment families in recent and fossil brachiopod shells. *Spectrochimica Acta Part A 208*, 7-84. https://doi.org/10.1016/j.saa.2018.09.050

Glaeser, G. & Paulus, H.F. 2015: *The Evolution of the Eye*. Springer, Cham. https://doi.org/10.1007/978-3-319-17476-1

Glass, K.E., Ito, S., Wilby, P.R., Sota, T., Nakamura, A., Bowers, C.R., Vinther, J., Dutta, S., Summons, R.E., Briggs, D.E.G. Wakamatsu, K. & Simon, J.D. 2012: Direct chemical evidence for eumelanin pigment from the Jurassic period. *Proceedings of the National Academy of Sciences 109*, 10218–10223. https://doi.org/10.1073/pnas.1118448109

Glass, K., Ito, S., Wilby, P.R., Sota, T., Nakamura, A., Bowers, C.R., Miller, K.E., Dutta, S., Summons, R.E., Briggs, D.E.G. Wakamatsu, K. & Simon, J.D. 2013: Impact of diagenesis and maturation on the survival of eumelanin in the fossil record. *Organic Geochemistry 64*, 29–37. https://doi.org/10.1016/j.orggeochem.2013.09.002

Gobo, W.V., Kunzmann, L., Ianuzzi., R., Barbosa dos Santos, T., Maria da Conceição, D., Nascimento Jr., D.R., Filho, W.F.S., Bachelier, J.B. & Coiffard, C. 2023: A new remarkable Early Cretaceous nelumbonaceous fossil bridges the gap between herbaceous aquatic and woody protealeans. *Scientific Reports 13*, 8978. https://doi.org/10.1038/s41598-023-33356-z

Gottfried, M.D. 1989: Earliest fossil evidence for protective pigmentation in an actinopterygian fish. *Historical Biology 3*, 79-83. https://doi.org/10.1080/08912968909386514

Grogan, E.D. & Lund, R. 1997: Soft tissue pigments of the Upper Mississippian chondrenchelyid, *Harpagofututor volsellorhinus* (Chondrichthyes, Holocephali) from the Bear Gulch Limestone, Montana, USA. *Journal of Paleontology 71*, 337-342. https://doi.org/10.1017/S002233600003924X

Gunasekaran, S. & Anbalagan, G. 2008: Spectroscopic study of phase transitions in natural calcite mineral. *Spectrochimica Acta Part A 69*, 1246–1251. https://doi.org/10.1016/j.saa.2007.06.036

Gunasekaran, S., Anbalagan, G. & Pandi, S. 2006: Raman and infrared spectra of carbonates of calcite structure. *Journal of Raman Spectroscopy 37*, 892–899. https://doi.org/10.1002/jrs.1518

Guzmán, J., Piovesan, E.K., Melo, R.M., Almeida-Lima, D., Jesus e Sousa, A. & Neumann V.H.M.L. 2023: Ostracoda and Foraminifera biostratigraphy and palaeoenvironmental evolution of the Aptian Santana Group, post-rift of the Araripe Basin, Brazil. *Gondwana Research 124*, 18-38. https://doi.org/10.1016/j.gr.2023.06.014

Heimhofer, U., Ariztegui, D., Lenniger, M., Hesselbo, S.P., Martill, D.M. & Rios-Netto, A.M. 2010: Deciphering the depositional environment of the laminated Crato fossil beds (Early Cretaceous, Araripe Basin, North-eastern Brazil). *Sedimentology 57*, 677–694, https://doi.org/10.1111/j.1365-3091.2009.01114.x

Haingård, M., Sjovall, P., Sylvestersen, R.L., Schultz, B.P. & Lindgren, J. 2021: Crypis in the pelagic real: Evidence from exceptionally preserved fossil fish larvae from the Eocene Stolleklint Clay of Denmark. *Palaeontology 64*, 805-815. https://doi.org/10.1111/pala.12574

Henriques, M.H.P., Reis, R.P.B.P., Fernandes, A.C.C.S., Srivastava, N.K. & Carvalho, I.S. 1998: Caracterização tafonómica das associações registradas de Dastilbe sp. do Membro Crato (Formação Santana; Bacia do Araripe - NE do Brasil; Cretácico). In: Actas do V Congresso Nacional de Geologia. Lisboa, Portugal: *Comunicações do Serviço Geológico de Portugal 84*, A201-A204.

Holden, C. 1997: Coloring Fossils. *Science 277*, 905. https://doi.org/10.1126/science.277.5328.905b

Hong, L. & Simon, J.D. 2007: Current understanding of the binding sites, capacity, affinity, and biological significance of metals in melanin. *Journal of Physical Chemistry B 111*, 7938-7947. https://doi.org/10.1021/jp071439h

Hu, D.-N., Simon, J.D. & Sarna, T. 2008: Role of ocular melanin in ophthalmic physiology and pathology. *Photochemistry and Photobiology 84*, 639-644. https://doi.org/10.1111/j.1751-1097.2008.00316.x

Huang, Z., Lui, H., Chen, X.K., Alajlan, A., McLean, D.I. & Zeng, H. 2004: Raman spectroscopy of *in vivo* cutaneous melanin. *Journal of Biomedical Optics 9*, 1198. https://doi.org/10.1117/1.1805553

Iniesto, M., Lopez-Archilla, A.I., Frenegal-Martínez, M., Buscalioni, A.D. & Guerrero, M.C. 2013: Involvement of microbial mats in delayed decay: an experimental essay on fish preservation. *Palaios 28*, 56-66. https://doi.org/10.2110/palo.2011.p11-099r

Iniesto, M., Laguna, C., Florin, M., Guerrero, M.C., Chicote, A., Buscalioni, A.D. & Lopez-Archilla, A.I. 2015a: The impact of microbial mats and their microenvironmental conditions in early decay of fish. *Palaios 30*, 792-801. https://doi.org/10.2110/palo.2014.086

Iniesto, M., Zeyen, N., López-Archilla, A.I., Bernard, S., Buscalioni, Á.D., Guerrero, M.C. & Benzerara, K. 2015b: Preservation in microbial mats: mineralization by a talc-like phase of a fish embedded in a microbial sarcophagus. *Frontiers in Earth Science 3*, 1-13. https://doi.org/10.3389/feart.2015.00051

Iniesto, M., Buscalioni, A.D., Carmen Guerrero, M., Benzerara, K., Moreira, D. & López-Archilla, A.I. 2016: Involvement of microbial mats in early fossilization by decay delay and formation of impressions and replicas of vertebrates and invertebrates. *Scientific Reports 6*, 25716. https://doi.org/10.1038/srep25716

Iniesto, M., Gutiérrez-Silva, P., Dias, J.J., Carvalho, I.S., Buscalioni, A.D. & López-Archilla, A.I. 2021: Soft tissue histology of insect larvae decayed in laboratory experiments using microbial mats: Taphonomic comparison with Cretaceous fossil insects from the exceptionally preserved biota of Araripe, Brazil. *Palaeogeography, Palaeoclimatology, Palaeoecology 564*, 110156. https://doi.org/10.1016/j.palaeo.2020.110156

Ito, S. & Wakamatsu, K. 2008: Chemistry of mixed melanogenesis—pivotal roles of dopaquinone. *Photochemistry and Photobiology 84*, 582-592. https://doi.org/10.1111/j.1751-1097.2007.00238.x

Ito, S., Wakamatsu, K., d'Ischia, M., Napolitano, A. & Pezzella, A. 2011: Structure of melanins. In: Borovanský, J. & Riley, P.A. (eds). *Melanin and Melanosomes: Biosynthesis, Biogenesis, Physiological, and Pathological Functions*. Wiley-Blackwell, 167-185. ISBN: 978-3-527-32892-5

Ito, S., Wakamatsu, K., Glass, K.E. & Simon, J.D. 2013: High-performance liquid chromatography estimation of cross-linking of dihydroxyindole moiety in eumelanin. *Analytical Biochemistry 434*, 221–225. https://doi.org/10.1016/j.ab.2012.12.005

Ito, S., Miyake, S., Maruyama, S., Suzuki, I., Commo, S., Nakanishi, Y. & Wakamatsu, K. 2017: Acid hydrolysis reveals a low but constant level of pheomelanin in human black to brown hair. *Pigment Cell & Melanoma Research 31*, 393-403. https://doi.org/10.1111/pcmr.12673

Ito, S. 2003: A chemist's view of melanogenesis. *Pigment Cell Research 16*, 230-236. https://doi.org/10.1034/j.1600-0749.2003.00037.x

Jarenmark, M., Sjövall, P., Ito, S., Wakamatsu, K. & Lindgren, J. 2021: Chemical evaluation of eumelanin maturation by ToF-SIMS and Alkaline Peroxide Oxidation HPLC Analysis. *International Journal of Molecular Sciences 22*, 161. https://doi.org/10.3390/ijms22010161

Jordan, D.S. 1910: Description of a collection of fossil fishes from the bituminous shales at Riacho Doce, State of Alagoas, Brazil. *Annals of the Carnegie Museum 7*, 23-34. https://doi.org/10.5962/p.78074

Justyn, N.M., Peteya, J.A., D'Alba, L. & Shawkey, M.D. 2017: Preferential attachment and colonization of the keratinolytic bacterium *Bacillus licheniformis* on black- and white-striped feathers. *The Auk 134*, 466-473. https://doi.org/10.1642/AUK-16-245.1

Kawamura, G. & Nishimura, W. 1980: S-potential from the retina of milkfish Chanos chanos Forsskål. *Bulletin of the Japanese Society of Scientific Fisheries 46*, 1421.

Kaxiras, E., Tsolakidis, A., Zonios, G. & Meng, S. 2006: Structural model of eumelanin. *Physical Review Letters 97*, 1-4. https://doi.org/10.1103/PhysRevLett.97.218102

Kim, Y.J., Wu, W., Chun, S.-E., Whitacre, J.F. & Bettinger, C.J. 2013: Biologically derived melanin electrodes in aqueous sodium-ion energy storage devices. *Proceedings of the National Academy of Sciences of USA 110*, 20912-20917. https://doi.org/10.1073/pnas.1314345110

Košťák, M., Schlögl, J., Culka, A., Tomašových, A., Mazuch, M. & Hudáčková, N. 2018: The unique preservation of *Sepia* soft tissues in the Miocene deposits (Serravalian, Vienna Basin): implications for the origin of microbodies in the fossil record. *Palaeogeography, Palaeoclimatology, Palaeoecology 493*, 111-118. https://doi.org/10.1016/j.palaeo.2018.01.005

Kouketsu, Y., Mizukami, T., Mori, H., Endo, S., Aoya, M., Hara, H., Nakamura, D. & Wallis, S. 2014: A new approach to develop the Raman carbonaceous material geothermometer for low-grade metamorphism using peak width. *Island Arc 23*, 33-50. https://doi.org/10.1111/iar.12057

Land, M.F. & Nilsson, D.-E. 2012: *Animal Eyes*. 2nd, Edition. Oxford University Press, Oxford.

Land, M.F. 2014: *The Eye: A Very Short Introduction*. Oxford University Press, Oxford.

Li, X., Zhou, Y., Zhao, T., He, X. & Pan, Y. 2024: Gradient maturation experiment on hairs implies taphonomic changes in fossil hairs. *Science China Earth Sciences 67*, 1-12. https://doi.org/10.1007/s11430-023-1461-8

Lindgren, J., Caldwell, MW., Konishi, T. & Chiappe, L.M. 2010: Convergent evolution in aquatic tetrapods: Insights from an exceptional fossil mosasaur. *PLoS One 5*, e11998. https://doi.org/10.1371/journal.pone.0011998

Lindgren, J., Uvdal, P., Sjövall, P., Nilsson, D.E., Engdahl, A., Schultz, B.P. & Thiel, V. 2012: Molecular preservation of the pigment melanin in fossil melanosomes. *Nature Communications 3*, 824-831. https://doi.org/10.1038/ncomms1819

Lindgren, J., Moyer, A., Schweitzer, M.H., Sjöll, P., Uvdal, P., Nilsson D.E., Heimdal, J., Engdhal, A., Gren, J.A., Schultz, B.P. & Kear, B.P. 2015: Interpreting melanin-based coloration through deep time: a critical review. *Proceedings of the Royal Society B 282*, 20150614. https://doi.org/10.1098/rspb.2015.0614

Lindgren, J., Kuriyama, T., Madsen, H., Sjövall, P., heng, W., Uvdal, P., Engdahl, A., Moyer, A.E., Gren, J.A., Kamazaki, N., Ueno, S. & Schweitzer, M.H. 2017: Biochemistry and adaptative colouration of an exceptionally preserved juvenile fossil sea turtle. *Scientific Reports 7*, 13324. https://doi.org/10.1038/s41598-017-13187-5

Lindgren, J., Sjövall, P., Thiel, V., Zheng, W., Ito, S., Wakamatsu, K., HAuff, R., Kear, B.P., Engdahl, A., Alwmark, C., Eriksson, M.E., Jarenmark, M., Sachs, S., Ahlberg, P.E., Marone, F., Kuriyama, T., Gustafsson, O., Malmberg, P., Thomen, A., Rodríguez-Meizoso, I., Uvdal, P., Ojika, M. & Schweitzer, M.H. 2018: Soft-tissue evidence for homeothermy and crypsis in a Jurassic ichthyosaur: *Nature 564*, 359–365. https://doi.org/10.1038/s41586-018-0775-x

Lindgren, J., Nilsson, D.-E., Sjövall, P., Jarenmark, M., Ito, S., Wakamatsu, K., Kear, B.P., Schultz, B.P., Sylvestersen, R.L., Madsen, H., LaFountain, Jr, J., Alwmark, C., Eriksson, M.E., Hall, S.A., Lindgren, P., Rodríguez-Meizoso, I. & Ahlberg, P. 2019: Fossil insect eyes shed light on trilobite optics and the arthropod pigment screen. *Nature 573*, 122-125. https://doi.org/10.1038/s41586-019-1473-z

Ma, X.-P. & Sun, X.-X. 2012: *Melanin: Biosynthesis, Functions and Health Effects*. Nova Science Publishers, New York.

Mackintosh, J.A. 2001: The antimicrobial properties of melanocytes, melanosomes and melanin and the evolution of black skin. *Journal of Theoretical Biology 211*, 101-113. https://doi.org/10.1006/jtbi.2001.2331

Manning, P.L., Edwards, N.P., Bergmann, U., Anné, J., Sellers, W.I., van Veelen, A., Sokaras, D., Egerton, V.M., Alonso-Mori, R., Ignatyev, K., van Dongen, B.E., Wakamatsu, K., Ito, S., Knoll, F. & Wogelius, R.A. 2019: Pheomelanin pigment remnants mapped in fossils of an extinct mammal. *Nature Communications 10*, 2250. https://doi.org/10.1038/s41467-019-10087-2

Marques, M.P.M., Mamede, A.P., Vassalo, A.R., Makhoul, C., Cunha, E., Gonçalves, D., Parker, S.F. & Batista de Carvalho, L.A.E. 2018: Heat-induced bone diagenesis probed by vibrational spectroscopy. *Scientific Reports 8*, 15935. https://doi.org/10.1038/s41598-018-34376-w

Martill, D.M., Bechly, G. & Loveridge, R.F. 2007*: The Crato fossil beds of Brazil*. Cambridge University Press, Cambridge. https://doi.org/10.1017/CBO9780511535512

McNamara, M.E., Van Dongen, B.E., Lockyer, N.P., Bull, I.D. & Orr, P.J. 2016: Fossilization of melanosomes via sulfurization. *Palaeontology 59*, 337-350. https://doi.org/10.1111/pala.12238

McNamara, M.E., Kaye, J.S., Benton, M.J., Orr, P.J., Rossi, V., Ito, S. & Wakamatsu, K. 2018: Non-integumentary melanosomes can bias reconstructions of the colours of fossil vertebrates. *Nature Communications 9*, 2878. https://doi.org/10.1038/s41467-018-05148-x

Melo, R.M., Guzmán, J., Almeida-Lima, D., Piovesan, E.K., Neumann, V.H.M. & Sousa, A.J. 2020: New marine data and age accuracy of the Romualdo Formation, Araripe Basin, Brazil. *Scientific Reports 10*, 15779. https://doi.org/10.1038/s41598-020-72789-8

Mendes, M., Bezerra, F.I. & Adami, K. 2021: Ecosystem structure and trophic network in the late Early Cretaceous Crato Biome. In: Iannuzzi, R., Rößler, R. & Kunzmann, L. (eds). *Brazilian Paleofloras*. Springer Cham, 1-19. https://doi.org/10.1007/978-3-319-90913-4_33-1

Meredith, P., Powell, B.J., Riesz, J., Nighswander-Rempel, S.P., Pederson, M.R. & Moore, E.G. 2006: Towards structure-property-function relationships for eumelanin. *Soft Matter 2*, 37–44. https://doi.org/10.1039/b511922g

Monnier, G., Frahm, E. Luo, B. & Missal, K. 2018: Development FTIR microspectroscopy for the analysis of animal-tissue residues on stone tools. *Journal of Archaeological Method and Theory 25*, 1-44. https://doi.org/10.1007/s10816-017-9325-3

Morais Neto, J.M., Hegarty, K. & Karner, G.D. 2006: Abordagem preliminar sobre paleotemperatura e evolução do relevo da Bacia do Araripe, Nordeste do Brasil, a partir da análise de

traços de fissão em apatita. *Boletim de Geociências da Petrobrás 14*, 113-119.

Morris, M.D. & Mandair, G.S. 2011: Raman assessment of bone quality. *Clinical Orthopaedics and Related Research 469*, 2160-2169. https://doi.org/10.1007/s11999-010-1692-y

Movasaghi, Z., Rehman, S. & ur Rehman, I. 2008: Fourier transform infrared (FTIR) spectroscopy of biological tissues. *Applied Spectroscopy Reviews 43*, 134-179. 10.1080/05704920701829043

Muscente, A.D., Czaja, A.D., Anné, L. & Colleary, C. 2018: Organic Matter in Fossils. In: White, W.M. (ed.). *Encyclopedia of Geochemistry, Encyclopedia of Earth Sciences Series*. Springer International Publishing, Cham, 1–5. https://doi.org/10.1007/978-3-319-39193-9_185-1

Ni, Q.Z., Sierra, B.N., La Clair, J.J. & Burkart, M.D. 2020: Chemoenzymatic elaboration of the Raper–Mason pathway unravels the structural diversity within eumelanin pigments. *Chemical Science 11*, 7836–7841. https://doi.org/10.1039/d0sc02262d

Nicol, J.A.C., Arnott, H.J. & Best, A.C.G. 1973: *Tapeta lucida* in bony fishes (Actinopterygii): a survey. *Canadian Journal of Zoology 53*, 69-81. https://doi.org/10.1139/z73-012

Nordén, K.K., Faber, J.W., Babarović, F., Stubbs, T.L., Selly, T., Schiffbauer, J.D., Štefanić, P.P., Mayr, G., Smithwick, F.M. & Vinther, J. 2018: Melanosome diversity and convergence in the evolution of iridescent avian feathers—implications for paleocolor reconstruction. *Evolution 73*, 15–27. https://doi.org/10.1111/evo.13641

Osés, G.L., Petri, S., Becker-Kerber, B., Romero, G.R., Rizzutto, M.A., Rodrigues, F., Galante, D, Silva, TF, Curado, JF, Rangel, EC, Ribeiro, R.P. & Pacheco, M.L.A.F. 2016: Deciphering the preservation of fossil insects: a case study from the Crato Member, Early Cretaceous of Brazil. *PeerJ 4*, e2756. https://doi.org/10.7717/peerj.2756

Osés, G.L., Petri, S., Voltani, C.G., Prado, G.M.E.M., Galante, D., Rizzutto, M.A., Rudnitzki, I.D., Silva, E.P., Rodrigues, F., Rangel, E.C., Sucerquia, P.A. & Pacheco, M.L.A.F. 2017: Deciphering pyritization-kerogenization gradient for fish soft-tissue preservation. *Scientific Reports 7*, 1468. https://doi.org/10.1038/s41598-017-01563-0

Parker, A.R. 2005: A geological history of reflecting optics. *Journal of the Royal Society Interface 2*, 1–17. https://doi.org/10.1098/rsif.2004.0026

Parry, L.A., Smithwick, F.M., Nordén, K.K., Saitta, E.T., Lozano-Fernandez, J., Tanner, A.R., Caron, J.B., Edgecombe, G.D., Briggs, D.E.G. & Vinther, J. 2018. Soft-bodied fossils are not simply rotten carcasses – toward a holistic understanding of exceptional fossil reservation: exceptional fossil preservation is complex and involves the interplay of numerous biological and geological processes. *BioEssays 40*, 1–11. https://doi.org/10.1002/bies.201700167

Perna, G. & Capozzi, V. 2012: Optical spectroscopy and structural properties of synthetic and natural eumelanin. In: Ma, X.-P. & Sun, X.-X. (eds). *Melanin: Biosynthesis, Functions, and Health Effects*. Nova Science Publishers, New York, 191-212.

Perna, G., Lasalvia, M., Gallo, C., Quartucci, G. & Capozzi, V. 2013: Vibrational characterization of synthetic eumelanin by means of Raman and surface enhanced Raman scattering. *The Open Surface Science Journal 5*, 1-8. https://doi.org/10.2174/1876531901305010001

Perna, G., Lasalvia, M. & Capozzi, V. 2016: Vibrational spectroscopy of synthetic and natural eumelanin. *Polymer International 65*, 1323-1330. https://doi.org/10.1002/pi.5182

Perry, C.T., Salter, M.A., Harborne, A.R., Crowley, S.F., Jelks, H.L. & Wilson, R.W. 2011: Fish as major carbonate mud producers and missing components of the tropical carbonate factory. *Proceedings of the National Academy of Sciences of USA 108*, 3865-3869. https://doi.org/10.1073/pnas.1015895108

Petsch, S. 2017: Kerogen. In: White, W. (ed.). *Encyclopedia of Geochemistry. Encyclopedia of Earth Sciences Series*. Springer, Cham, 1-5. https://doi.org/10.1007/978-3-319-39193-9_163-1

Pinheiro, F.L., Prado, G., Ito, S., Simon, J.D., Wakamatsu, K., Anelli, L.E., Andrade, J.A.F.G. & Glass, K.E. 2019. Chemical characterization of pterosaur melanin challenges color inferences in extinct animals. *Scientific Reports 9*, 15947. https://doi.org/10.1038/s41598-019-52318-y

Polk, M.A.R., Carvalho, M.S.S., Miguel, R. & Gallo, V. 2015: *Guia de identificação de peixes fósseis das formações Crato e Santana da Bacia do Araripe*. CPRM, Rio de Janeiro.

Powell, B.J., Baruah, T., Bernstein, N., Brake, K., McKenzie, R.H., Meredith, P. & Pederson, M.R. 2004: A first-principles density-functional calculation of the electronic and vibrational structure of the key melanin monomers. *Journal of Chemical Physics 120*, 8608–8615. https://doi.org/10.1063/1.1690758

Prampolini, G., Cacelli, I. & Ferretti, A. 2015: Intermolecular interactions in eumelanins: A computational bottom-up approach. I. small building blocks. *RSC Advances 5*, 38513–38526. https://doi.org/10.1039/c5ra03773e

Prado, G., Arthuzzi, J.C.L., Osés, G.L., Callefo, F., Maldanis, L., Sucerquia, P., Becker-Kerber, B., Romero, G.R., Quiroz-Valle, F.R., Galante, D. (2021). Synchrotron radiation in palaeontological investigations: Examples from Brazilian fossils and its potential to South American palaeontology. Journal of South American Earth Sciences, 108, 102973. https://doi.org/10.1016/j.jsames.2020.102973

Price A.C., Weadick, C.J., Shim, J. & Rodd, F.H. 2008: Pigments, patterns, and fish behaviour. *Zebrafish 5*, 297-307. https://doi.org/10.1089/zeb.0551

Ribeiro, A.C., Ribeiro, G.C., Varejão, F.G., Battirola, L.D., Pessoa, E.M., Simões, M.G., Warren, L.V., Riccomini, C. & Poyato-Ariza, F.M. 2021: Towards an actualistic view of the Crato *Konservat-Lagerstätte* paleoenvironment: a news hypothesis as an Early Cretaceous (Aptian) equatorial and semi-arid wetland. *Earth Science Reviews 214*, 103573. https://doi.org/10.1016/j.earscirev.2021.103573

Rios-Netto, A.M., Regali, M.S.P., Carvalho, I.S. & Freitas, F.I. 2012: Palinoestratigrafia do intervalo Alagoas da Bacia do Araripe, Nordeste do Brasil. *Revista Brasileira de Geociências 42*, 331–342, https://doi.org/10.25249/0375-7536.2012422331342

Robbins, L.L. & Blackwelder, P.L. 1992: Biochemical and ultrastructural evidence for the origin of whitings: a biologically induced calcium carbonate precipitation mechanism. *Geology 20*, 464-468. https://doi.org/10.1130/0091-7613(1992)020<0464:BAUEFT>2.3.CO;2 1435

Rogers, C.S., Astrop, T.I., Webb, S.M., Ito, S., Wakamatsu, K. & McNamara, M.E. 2019: Synchrotron X-ray absorption spectroscopy of melanosomes in vertebrates and cephalopods: Implications for the affinity of *Tullimonstrum*. *Proceedings of the Royal Society B 286*, 20191649. https://doi.org/10.1098/rspb.2019.1649

Roldán, M.L., Centeno, S.A. & Rizzo, A. 2014: An improved methodology for the characterization and identification of *Sepia* in words of art by normal Raman and SERS, complemented by FTIR, Py-GC/MS, and XRF. *Journal of Raman Spectroscopy 45*, 1160-1171. https://doi.org/10.1002/jrs.4620

Rossi, V., Webb, S.M. & McNamara, M.E. 2020: Hierarchical biota-level and taxonomic controls on the chemistry of fossil melanosomes revealed using synchrotron X-ray fluorescence. *Scientific Reports 10*, 8970. https://doi.org/10.1038/s41598-020-65868-3

Rossi, V., Webb, S.M. & McNamara, M. 2021: Maturation experiments reveal bias in the chemistry of fossil melanosomes. *Geology 49*, 784-788. https://doi.org/10.1130/G48696.1

Rossi, V., Unitt, R. & McNamara, M. 2024: A new non-destructive method to decipher the origin of organic matter in fossils using Raman spectroscopy. *RSC Advances 14*, 26747-26759. https://doi.org/10.1039/D4RA04364B

Rossi, V., Unitt, R., McNamara, M., Zorzin, R. & Carnevale, G. 2022: Skin patterning and internal anatomy in a fossil moonfish from the Eocene Bolca *Lagerstätte* illuminate the ecology of ancient reef fish communities. *Palaeontology 65*, e12600. https://doi.org/10.1111/pala.12600

Roy, A., Pittman, M., Saitta, E.T., Kaye, T.G. & Xu, X. 2020a: Recent advances in amniote palaeocolour reconstruction and

a framework for future research. *Biological Reviews 95*, 1–29. https://doi.org/10.1111/brv.12552

Roy, A., Rogers, C.S., Clements, T., Pittman, M., Habimana, O., Martin, P. & Vinther, J. 2020b: Fossil microbodies are melanosomes: evaluating and rejecting the 'fossilized decay-associated microbes' hypothesis. In: Pittman, M. & Xu, X. (eds). Pennaraptoran theropod dinosaurs: past progress and new frontiers. *Bulletin of the American Museum of Natural History 440*, 251-276. https://doi.org/10.1206/0003-0090.440.1.1

Roy, A., Pittman, M., Kaye, T. & Saitta, E. 2023: Sediment-encased pressure-temperature maturation experiments elucidate the impact of diagenesis on melanin-based fossil color and its paleobiological implications. *Paleobiology 49*, 712-732. https://doi.org/10.1017/pab.2023.11

Różanowska, M., Sarna, T., Land, E.J. & Truscott, T.G. 1999: Free radical scavenging properties of melanin. *Free Radical Biology and Medicine 26*, 518–525. https://doi.org/10.1016/S0891-5849(98)00234-2

Salgado, F.L.K. & Carvalho, I.S. 2023: Cannibal predatory habits and their relationships with body shape and swimming pattern in the Cretaceous fish *Dastilbe crandalli* Jordan, 1910 from the Araripe Basin, Northeastern Brazil. *Cretaceous Research 152*, 105685. https://doi.org/10.1016/j.cretres.2023.105685

Santos Filho, M.A.B., Ceolin, D., Fauth, G. & Lima, F.H.O. 2023: Ostracods from the Barbalha and Crato formations, Aptian of the Araripe Basin, northeast Brazil. *Zootaxa 5319*, 332–350. https://doi.org/10.11646/zootaxa.5319.3.2

Schmidt, S.Y. & Peisch, R.D. 1986: Melanin concentration in normal human retinal pigment epithelium. Regional variation and age-related reduction. *Investigative Ophthalmology & Visual Science 27*, 1063-1067. PMID: 3721785

Schneider, C.A., Rasband, W.S. & Eliceiri, K.W. 2012: NIH Image to ImageJ: 25 years of image analysis. *Nature Methods 9*, 671–5. https://doi.org/10.1038/nmeth.2089

Smith, E. & Dent, G. 2005: *Modern Raman Spectroscopy – A Practical Approach*. *John Wiley & Sons*, LOCATION.

So, R.T., Blair, N.E. & Masterson, A.L. 2020: Carbonate mineral identification and quantification in sediment matrices using diffuse reflectance infrared Fourier transform spectroscopy. *Environmental Chemistry Letters 18*, 1725–1730. https://doi.org/10.1007/s10311-020-01027-4

Solano, F. 2014: Melanins: skin pigments and much more-types, structural models, biological functions, and formation routes. *New Journal of Science 2014*, 498276. https://doi.org/10.1155/2014/498276

Storari, A.P., Osés, G.L., Almeida-Lima, D.S., Rizzutto, M.A., Bantim, R.A.M., Lima, F.J., Rodrigues, T. & Sayão, J.M. 2024: Exceptionally well-preserved orthopteran proventriculi from the Cretaceous Crato Formation of Brazil. *Journal of South American Earth Sciences 133*, 104737. https://doi.org/10.1016/j.jsames.2023.104737

Tanaka, G., Parker, A.R., Hasegawa, Y., Siveter, D.J., Yamamoto, R., Miyashita, K., Takahashi, Y., Ito , S., Wakamatsu, K., Mukuda, T., Matsuura, M., Tomikawa, K., Furutani, M., Suzukim K. & Maeda, H. 2014: Mineralized rods and cones suggest colour vision in a 300 Myr old fossil fish. *Nature Communications 5*, 5920. https://doi.org/10.1038/ncomms6920

Tanaka, G., Zhou, B., Zhang, Y., Siveter, D.J. & Parker, A.E. 2017: Rods and cones in an enantiornithine bird eye from the Early Cretaceous Jehol Biota. *Heliyon 3*, e00479. https://doi.org/10.1016/j.heliyon.2017.e00479

Tran, M.L., Powell, B.J. & Meredith, P. 2006: Chemical and structural disorder in eumelanins: A possible explanation for broadband absorbance. *Biophysical Journal 90*, 743–752. https://doi.org/10.1529/biophysj.105.069096

Umamaheswaran, R., Dutta, S. & Kumar, S. 2021: Elucidation of the macromolecular composition of fossil biopolymers using Py-GCxGC-TOFMS. *Organic Geochemistry 151*, 104139. https://doi.org/10.1016/j.orggeochem.2020.104139

Umamaheswaran, R., Dutta, S., Singh, H. & Kumar, S. 2022: Pyrolisis-GCxGC-TOFMS as a tool for distinguishing the macromolecular structure of nitrogen-bearing animal biopolymers in fossil tissues. *Journal of Analytical and Applied Pyrolysis 161*, 105362. https://doi.org/10.1016/j.jaap.2021.105362

Varejão, F.G., Warren, L. V., Simões, M.G., Fursich, F.T., Matos, S.A. & Assine, M.L. 2019: Exceptional preservation of soft tissues by microbial entombment: Insights into the taphonomy of the Crato *Konservat-Lagerstätte*. *Palaios 34*, 331–348. https://doi.org/10.2110/palo.2019.041

Vinther, J., Briggs, D.E.G. Prum, R.O. & Saranathan, V. 2008: The colour of fossil feathers. *Biology Letters 4*, 522–525. https://doi.org/10.1098/rsbl.2008.0302

Vinther, J. 2020: Reconstructing vertebrate paleocolor. *Annual Reviews of Earth and Planetary Sciences 48*, 345-375. https://doi.org/10.1146/annurev-earth-073019-045641

Wakamatsu, K., Nagao, A., Watanabe, M., Nakao, K. & Ito, S. 2017: Pheomelanogenesis is promoted at a weakly acidic pH. *Pigment Cell & Melanoma Research 30*, 372-377. https://doi.org/10.1111/pcmr.12587

Walsh, P. J., Blackwelder, P., Gill, KA., Danulat, E. & Mommsen, T.P. 1991: Carbonate deposits in marine fish intestines: a new source of biomineralization. *Limnology and Oceanography 36*, 1227-1232. https://doi.org/10.4319/lo.1991.36.6.1227

Warren, L.V., Varejão, F.G., Quaglio, F., Simões, M.G., Fursich, F.T., Poiré, D.G., Catto, B. & Assine, M.L. 2017: Stromatolites from the Aptian Crato Formation, a hypersaline lake system in the Araripe Basin, northeastern Brazil. *Facies 63*, 1–19. https://doi.org/10.1007/s10347-016-0484-6

Wasmeier, C., Hume, A.N., Bolasco, G. & Seabra, M.C. 2008: Melanosomes at a glance. *Journal of Cell Science 12*1, 3995–3999. https://doi.org/10.1242/jcs.040667

Watt, A.A.R., Bothma, J.P. & Meredith, P. 2009: The supramolecular structure of melanin. *Soft Matter 5*, 3754. https://doi.org/10.1039/b902507c

Wogelius, R.A., Manning, P.L., Barden, H.E., Edwards, N.P., Webb, S.M., Sellers, W.I., Taylor, K.G., Larson, L., Dodson, P., You, H., Da-qing, L. & Bergmann, U. 2011: Trace metals as biomarkers for eumelanin pigment in the fossil record. *Science 333*, 1622-1626. https://doi.org/10.1126/science.1205748

Xiao, M., Chen, W., Li, W., Zhao, J., Hong, Y., Nishiyama, Y., Miyoshi, T., Shawkey, M.D. & Dhinojwala, A. 2018: Elucidation of the hierarchical structure of natural eumelanins. *Journal of The Royal Society Interface 15*, 20180045. https://doi.org/10.1098/rsif.2018.0045